REPUBLIC OF TÜRKİYE
ADANA ALPARSLAN TÜRKEŞ SCIENCE AND TECHNOLOGY UNIVERSITY

GRADUATE SCHOOL
AEROSPACE ENGINEERING DEPARTMENT

THE EFFECT OF PARTIAL FLEXIBILITY ON AERODYNAMIC PERFORMANCE OF FINITE WING

ALI EMIRHAN EROGLU

M.Sc.

ADANA 2025

REPUBLIC OF TÜRKİYE
ADANA ALPARSLAN TÜRKEŞ SCIENCE AND TECHNOLOGY UNIVERSITY

GRADUATE SCHOOL
AEROSPACE ENGINEERING DEPARTMENT

THE EFFECT OF PARTIAL FLEXIBILITY ON AERODYNAMIC PERFORMANCE OF FINITE WING

ALI EMIRHAN EROGLU

M.Sc.

THESIS ADVISOR
ASSOC. PROF. DR. TAHIR DURHASAN

ADANA, 2025

ÖZET

KISMİ ESNEKLİĞİN SONLU KANATLARIN AERODİNAMİK PERFORMANSI ÜZERİNDEKİ ETKİSİ

Ali Emirhan EROĞLU
Yüksek Lisans, Havacılık ve Uzay MühendisliğiAnabilim Dalı
Danışman: Doç. Dr. Tahir DURHASAN
Temmuz 2025, 75 sayfa

Bu tez çalışmasında, düşük Reynolds sayılı akış rejimlerinde çalışan NACA 0018 tipi bir kanat üzerine kısmi esnek kaplama uygulanarak aerodinamik performansa olan etkileri deneysel olarak incelenmiştir. Çalışmada kullanılan esnek yüzey, kanadın belirli bir chord uzunluğu boyunca yerleştirilmiş lateks malzemeden oluşmakta ve kanadın farklı açıklık oranlarına sahip dört versiyonu ile test edilmiştir.

Rüzgâr tüneli testlerinde; taşıma (C_L) ve sürükleme (C_D) katsayıları $3 \times 10^4 \leq Re \leq 10 \times 10^4$ aralığında 4 farklı Re koşulunda ölçülmüş, ayrıca yüzey yağ ve ip (tuft) ile akış görselleştirme deneyleri gerçekleştirilmiştir. Elde edilen bulgular, kısmi esnek yüzeyin özellikle düşük Reynolds sayılarında laminer ayrılma balonunu (LSB) baskıladığını, stall açısını geciktirdiğini ve taşıma katsayısını artırarak kanadın genel aerodinamik performansını iyileştirdiğini ortaya koymuştur. Ancak Reynolds sayısı arttıkça bu etkinin azaldığı gözlemlenmiştir.

Bu sonuçlar, pasif akış kontrol tekniklerinin optimize edilmesinde kısmi esnek yüzeylerin potansiyel faydalarını göstermesi açısından literatüre katkı sunmaktadır.

Anahtar Kelimeler: Aerodinamik, Esnek Kanat, Laminer Ayrılma Kabarcığı, İnsansız Hava Aracı, Pasif Akış Kontrolü

ABSTRACT

THE EFFECT OF PARTIAL FLEXIBILITY ON AERODYNAMIC PERFORMANCE OF FINITE WING

Ali Emirhan EROGLU
M.Sc., Department of Aerospace Engineering

Supervisor: Assoc. Prof. Dr. Tahir DURHASAN
July 2025, 75 pages

In this thesis, the aerodynamic effects of partially flexible surface coverage applied to a NACA 0018 airfoil operating in low Re regimes were experimentally investigated. The flexible surface, made of latex material, was placed along a specific chordwise region of the wing, and four different wings with varying spanwise flexibility ratios were tested.

Wind tunnel experiments were conducted in the Re range of 3×10^4 to 10×10^4, measuring lift (C_L) and drag (C_D) coefficients. Additionally, surface oil and tuft flow visualization techniques were used to analyze flow structures. The findings revealed that the partially flexible surface significantly suppressed the laminar separation bubble (LSB), delayed stall, and enhanced lift coefficient, thereby improving aerodynamic efficiency, particularly at lower Re. However, the effectiveness of the flexible surface diminished as the Re increased.

These results contribute to the literature by demonstrating the potential of partial flexibility in optimizing passive flow control methods for UAV applications.

Keywords: Aerodynamics, Flexible Wing, Laminar Separation Bubble, UAV, Passive Flow Control

ACKNOWLEDGEMENTS

This thesis would not have been possible without the guidance and support of many individuals. I would like to express my sincere gratitude to all those who have contributed to this journey.

First and foremost, I would like to extend my deepest and most sincere gratitude to my supervisor, Assoc. Prof. Dr. Tahir DURHASAN, for his invaluable guidance, unwavering support, and insightful feedback throughout this research. His expertise, encouragement, and patience were instrumental in shaping this thesis from its initial stages to its completion. I am profoundly grateful for their mentorship and for inspiring me to strive for academic excellence.

I also would like to thank to Asst. Prof. Dr. Muhammet Murat AKSOY for their supporting and encourage. In addition I am deeply grateful to my colleagues Javad RASHID JAFERI and Buse EROL in the lab. Their teamwork and positive energy created a wonderful working environment, and I truly value the companionship we shared.

I would also like to extend my heartfelt thanks to my beloved family, especially to like my parents, Yasemin EROGLU and Nihat EROGLU. Thank you for your endless love, understanding, and unwavering belief in me. I cannot pass my sister Fatmanur EROGLU which always try to make me laugh when I get stress. I also thank to my little sister Elif EROGLU who I feel the hope when I look her. Your emotional support and encouragement have been the foundation of my perseverance, and this achievement is as much yours as it is mine.

Last but not least, I am grateful to my wonderful friends Erdinc ASLAN, Yusuf YAZGAN, and Alican CILINGIR for their friendship, moral support, and for providing much-needed breaks and laughter during the most challenging times. Your friendship was a constant source of motivation and helped me maintain my sanity throughout this process.

This thesis was supported by TUBITAK with project number 223M340.

TABLE OF CONTENTS

LIST OF FIGURES

LIST OF ABBREVIATIONS

UAV	: Unmanned Air Vehicle
MAV	: Micro Air Vehicle
Re	: Reynolds Number
LSB	: Laminar Separation Bubble
C_L	: Lift Coefficient
C_D	: Drag Coefficient
C_L/C_D	: Lift-to-Drag Ratio
AR	: Aspect Ratio
AFC	: Active Flow Control
PFC	: Passive Flow Control
LEV	: Leading Edge Vortex
SMA	: Shape Memory Alloy
SJA	: Synthetic Jet Actuator
PSJA	: Plasma Based Synthetic Jet Actuator
FSI	: Fluid Structure Interaction
LE	: Leading Edge
TE	: Trailing Edge
MHD	: Magnetohydrodynamic
CJA	: Continuous Jet Actuator
CFD	: Computational Fluid Dynamics
WAVT	: Vertical Axis Wind Turbine
PIV	: Particle Image Velocimetry

LIST OF SYMBOLS

c	**:** Chord
s	**:** Span
ρ	**:** Fluid density (kg/m³)
V	**:** Flow velocity (m/s)
μ	**:** Dynamic viscosity (Pa·s or N·s/m²)
D	**:** Characteristic dimension (wing chord, m)
ν	**:** μρ\nu = kinematic viscosity (m²/s)
ψ	**:** Angle between slot axis and chord normal
E	**:** Young’s Modulus

1. INTRODUCTION

Studies on the aerodynamic performance of the wings have been attracting much attention with the increasing use of unmanned aerial vehicles (UAVs) and micro air vehicles (MAVs) in civil and military areas as well as increasing energy demands. Flow regimes can be classified depending on the Reynolds number (Re) and UAVs, MAVs and small-scale wind turbines operate in low Re regime (Re < 10^5). The main flow characterictics of low Re regimes is formation of laminar separation bubble (LSB) on the wings. The presence of the bubble can induce a strong suction peak near the leading edge (LE) and significantly affects the aerodynamic performance of the airfoil [1,2]. To investigate the formation of LSB and its adverse results on aerodynamic efficiency perspective, various studies have been conducted [3-6]. On the other hand, various flow control techniques classified as active and passive have been applied to increase the aerodynamic efficiency of the wing. The principle of active flow control (AFC) techniques is based on the use of external energy, while passive flow control (PFC) techniques are based on adding devices to the flow or modification of geometry. Some illustrative examples for AFC techniques can be given as plasma actuators [7], synthetic jets [8], magnetic fields [9], etc. On the other hand, it can be given as an example for PFC techniques such as control rods [10,11], vortex generators [12,13], slots [14], etc. Flow control techniques are extensively categorized in the existing literature [15].

Besides well-known flow control techniques, advancements in material science lead to more efficient, adaptable, and high-performing wings. For example, smart materials such as shape memory alloys (SMAs), piezoelectric actuators, and variable stiffness structures not only increase aerodynamic performance but also enable maneuverability and flight control. Furthermore, flexible wings are utilized in aerospace industry since they provide significant benefits including low weight, cost-effectiveness, fight agility, reduced cost, and excellent performance [15-20]. The flexibility of wing surfaces contributes to aerodynamic efficiency and flight stability by allowing the wing shape to adapt spontaneously to free-flow conditions. However, this typically results in a complex fluid–structure interaction (FSI) problem that is strongly coupled and related to the structural dynamics and aerodynamics of flexible wings.

1.1. Low Reynolds Number Aerodynamic

Recent years have witnessed significant advancements in low-speed aircraft, high-altitude long-endurance UAVs, and high-performance MAVs. One of the primary design challenges for these vehicles is accurately assessing the impact of low Reynolds numbers. The wing aerodynamics at low Re for fixed-wing UAV and wind turbines and rotary or flapping-wing MAV have not yet been fully understood. The unsteady aerodynamic behavior that occurs especially in low Re flow conditions continues to be an important issue that attracts the attention of researchers [21]. The Re defined as the ratio of inertial to viscous forces in a fluid as given in Equation 1.1, plays a crucial role in determining aerodynamic behavior. For aerospace applications as external flow, Re around 10^5 are typically considered ‘low’ while conventional aircraft operate at Re of 10^6 or higher [22]. At low Re, viscous effects dominate, significantly influencing drag, lift-to-drag ratio, and overall aerodynamic performance [23]. Low Re flows often result in nonlinear aerodynamic characteristics and unsteady flow features, such as laminar separation bubbles (LSBs), which can degrade performance.

$$\mathrm{Re} = \frac{\rho \cdot V \cdot L}{\mu} \tag{1.1}$$

where L represents characteristic length of the airfoil, μ represents dynamic viscosity of the air, *V* represents free-stream velocity, ρ represents density of the air.

At low Reynolds flow;

- Flow is generally laminar over most of the wing surface.
- The boundary layer is thin and smooth.
- Flow is sensitive to surface roughness and external disturbances.
- The flow can separate easily from the surface due to low momentum in the boundary layer.
- At very low Re, the flow is often described as “creeping flow” or “viscous dominated.”
- Flow separation can occur early along the wing, causing a sharp drop in lift and a significant increase in drag.

Numerous examples of low and very low Re number flows can be found both in engineering applications and in nature. Figure 1.1 illustrates some of these examples by presenting a comparison of flight speed and chord Re, including cases like micro aerial vehicles, unmanned aerial vehicles, as well as birds and insects.

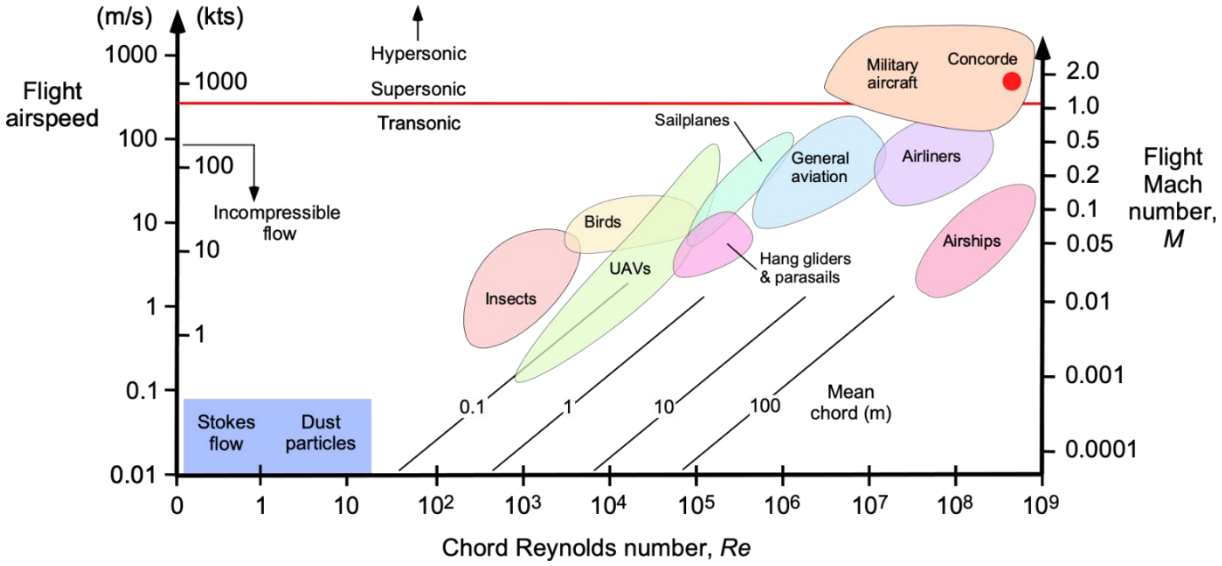

Figure 1.1. Classification of flying objects over a relation of chord and Re [24]

The primary distinction between different flying objects is related to the reduction in wing chord length. When the chord length decreasing, Re number of flows decreases too. The viscous region in the flow around the wing is very large and the viscous forces in the flow are more dominant than the inertial forces at low Reynolds flow That causes flow separation to occur earlier compared to flows at higher Reynolds.

1.1.1 Laminar separation bubble

In low Reynolds flows, the flow is unsteady. In this Re range, flow separation may occur due to the increase in the angle of attack on the wing. As seen in Figure 1.2, at the moment when the flow separation occurs, the laminar flow turns into turbulent flow and this region is called the transition region. There are three main sections explaining the flow separation. First, the flow accelerates and the pressure drops where the air accelerates. Then, the flow slowly loses momentum as the adverse pressure increases. At the end of this stage, the flow begins to separate. In the last section, the pressure remains constant after the flow separation. With the transition to turbulent flow, the energized flow separates from the laminar boundary layer and then transitions to turbulence, which increases the energy of the flow [25].

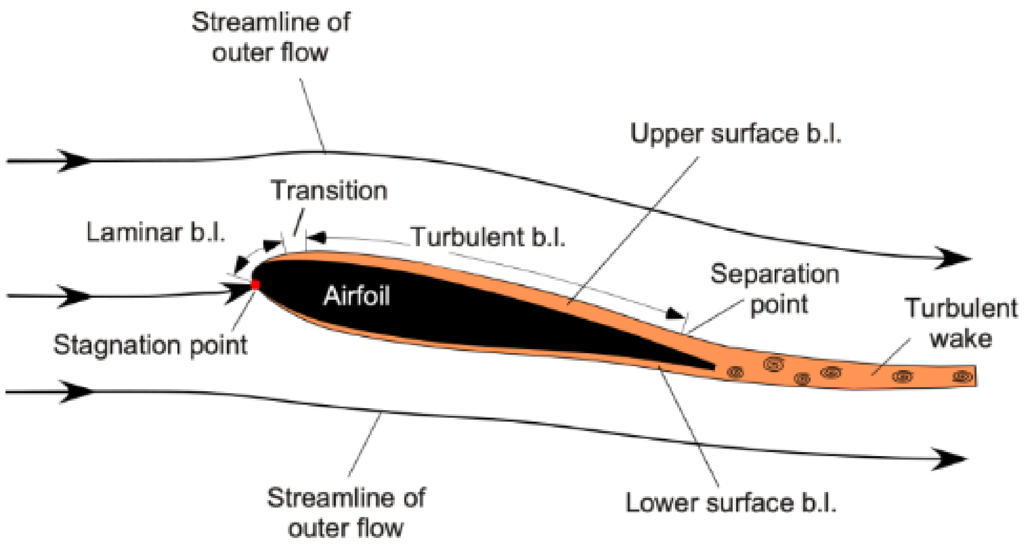

Figure 1.2. Flow Separation on Airfoil [26]

The turbulent flow reattaches to the fuselage surface and a reverse flow region is formed. The pressure coefficient distribution above the airfoil shows the presence of a hump as shown in Figure 1.3. The beginning and end of this hump reveal the separation and reattachment of the flow. Because of the viscous forces are dominant then inertial forces, laminar flow begins to deteriorate rapidly as it progresses from the LE to the TE. In the transition region to turbulence, the flow separates due to adverse pressure gradients and viscous forces. However, after passing into turbulence, it reattaches to the surface and forms an LSB. There are backflow and reverse velocity profiles in the inner region of the bubble [27].

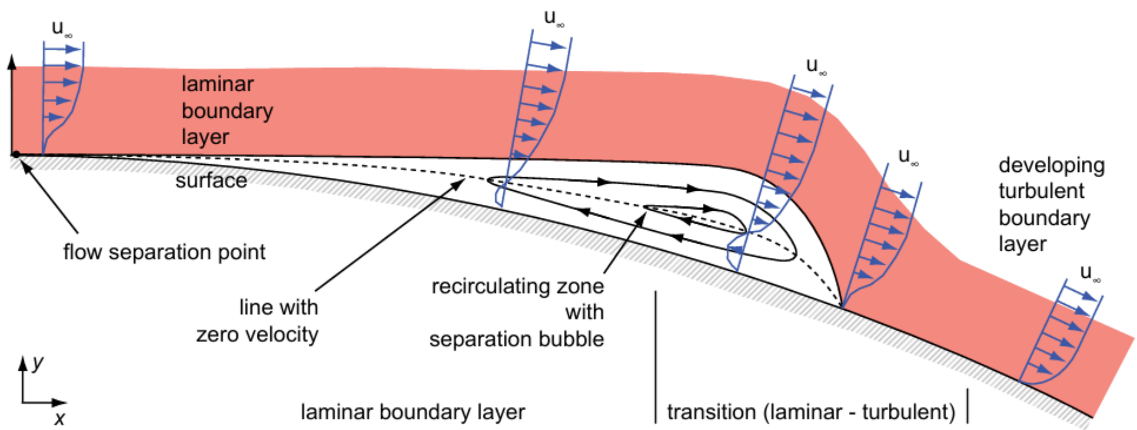

Figure 1.3. Laminar separation bubble [28]

The formation of this separation bubble causes instability and vibrations in aircraft flying at low Re, which has a negative effect on aerodynamic performance [29].

The main reason for the formation of the adverse pressure gradient is the no-slip condition between the surface and the fluid. According to the no-slip condition principle, shear stress occurs depending on the viscosity of the fluid, as given in Equation 1.2.

$$\tau = \mu\left(\frac{du}{dy}\right) \tag{1.2}$$

τ represents the shear force, μ represents the dynamic viscosity of the fluid, and u is freestream velocity.

The location and size of the bubble are a function of the angle of attack, flow disturbances, wing geometry, and Re. As the angle of attack increases, the small-sized LSB moves in the flow direction and becomes smaller. In the pressure distribution inside such a bubble, a small constant pressure region can be seen. The separation point continues to advance towards the LE as the angle of attack increases [30].

1.1.2 Finite wing

The main difference of finite and infinite wing is the existing of tip vortex. As illustrated in Figure 1.4, the flow over a finite wing generates a wake structure downstream, characterized by trailing vortices originating from the wingtips. These vortices resemble horizontal tornadoes, exhibiting strong rotational flow – referred to as induced velocities – particularly concentrated near the core and often extending beyond the wingspan. The vortices are significantly affecting aerodynamics of air vehicles with left in the path behind the wing, reducing lift and increasing its drag.

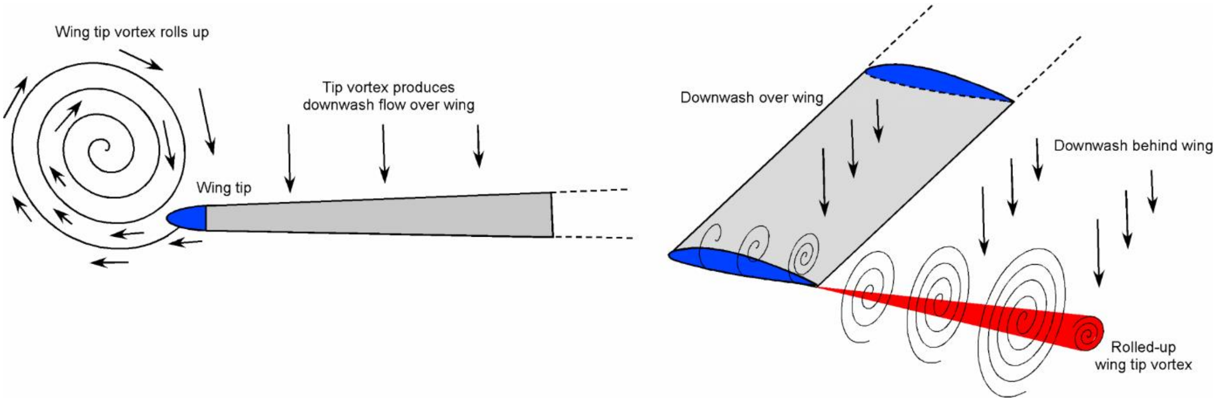

Figure 1.4. The wing tip vortices [31]

In the field of aerodynamics, studies on LSBs have predominantly concentrated on two-dimensional airfoil geometries. However, the finite wings, additional three-dimensional influences come into play, significantly affecting the characteristics of separation bubbles, particularly under low Re conditions [32]. This phenomenon is especially important for practical applications like UAVs, MAVs, and other small-scale aircraft, which typically operate within this flow regime.

For finite wings, spanwise flow occurring near the wing root and tips alters the formation of the separation bubble, usually causing it to thicken around the midspan and become thinner towards the tips [33]. While the flow close to the root is affected by turbulence from boundary layers, leading to an earlier transition to turbulence, the region near the tip tends to resist laminar separation, delaying the transition process. As a result, the laminar separation bubble exhibits variations in size and behavior along the span of the wing.

1.2. Flow Control Techniques

Flow separation, as discussed earlier, is the failure of the flow around an airfoil to adhere to the surface due to the loss of airflow momentum due to increasing adverse pressure gradients and no-slip conditions. As the angle of attack increases, the separation point on the intake surface gradually shifts toward the LE of the airfoil. In addition, at higher angles of attack, loss of traction occurs, resulting in a sudden decrease in lift and a rapid increase in drag. Figure 1.5 illustrates the effects of flow separation on an airfoil.

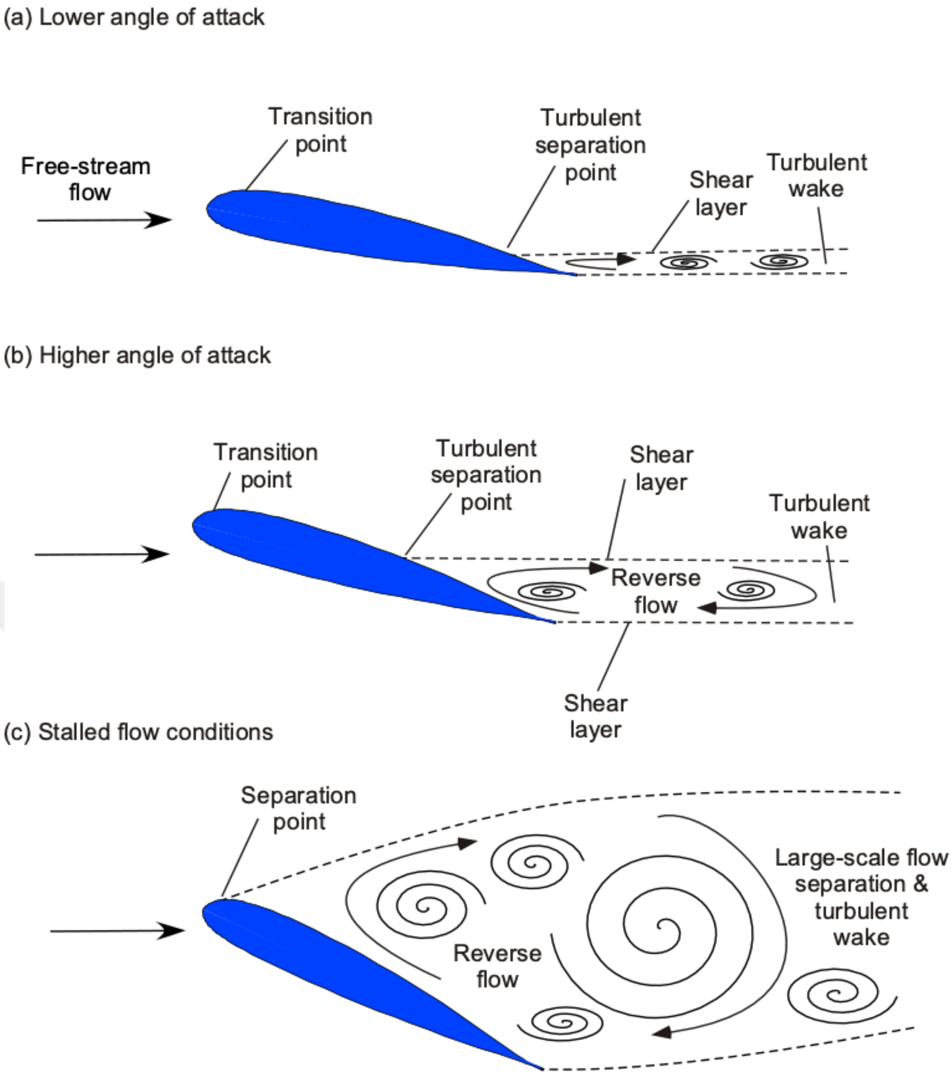

Figure 1.5. Stages of flow separation on airfoil [34]

In addition, when an airfoil operates at sufficiently high Re, flow separation results in the formation of a periodic vortex shedding. This regime results in a significant pressure drop at the TE of the airfoil. Furthermore, vortex shedding causes strong structural vibrations, resonance, and fluctuations in lift and drag forces [35]. Although increment of turbulence can increase heat transfer, the primary disadvantages of vortex shedding include excessive vibrations and acoustic noise [36]. Due to these adverse effects, flow control has become a critical area of interest for researchers aiming to reduce or eliminate undesirable aerodynamic behaviors. To prevent or minimize these consequences, flow control techniques have been studied since the discovery of the boundary layer by Prandtl [37]. The purpose of flow control can vary according to the desired goals, such as reducing drag or lift, disturbing laminar flow, improving heat transfer, suppressing vortex-induced vibration, and suppressing flow-induced noise, etc. Accordingly, depending on the intended aerodynamic outcome, flow control can be utilized to manipulate the transition between laminar and turbulent regimes, adjust turbulence intensity, or manage flow separation [38]. The fundamental concept behind such techniques involves modifying either the surface geometry or the wake characteristics to influence the behavior of boundary and shear layers. In this context, various control techniques have been applied to regulate the vortex shedding around airfoils. These control techniques are divided into two main groups: passive flow control (PFC) and active flow control (AFC). While AFC require external energy, PFC do not require any energy. Therefore, PFC techniques are easier to apply than AFC techniques.

Classification of flow control methods and some implementation shown in Figure 1.6.

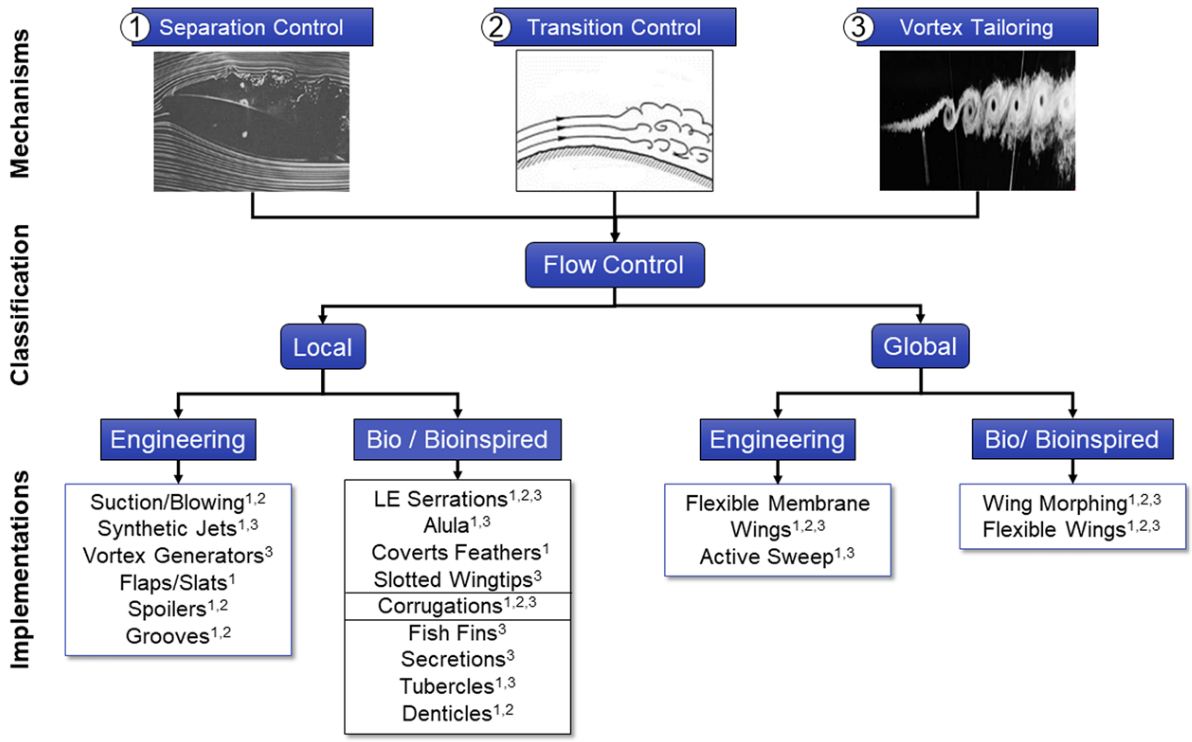

Figure 1.6. Classification of flow control methods and their implementations [39]

Generally, PFC techniques are cost-effective, structurally simple, and require no additional energy input. Due to these advantages, extensive research has been conducted in this field, with experts focusing on numerical simulations, experimental studies, and real-world applications of PFC.

1.2.1 Passive flow control

PFC techniques are widely used for flow control applications. The main reasons why they are preferred over active flow control techniques are; being easier to implement, lower cost and more stable. Examples of passive flow control techniques are widely encountered in offshore research and marine hydraulics, as well as in the aviation and automotive industries. PFC techniques control vortex shedding by changing the geometry of the airfoil or by adding additional devices to the flow boundary. It is dramatically important that determining the flow phenomena at low Re to design the widespread airfoils in the micro aircraft and wind turbines [40]. Flow control methods like these are commonly used to enhance the aerodynamic performance of flight vehicles by altering the flow behavior within the boundary layer, as controlling the flow is an effective approach to regulate mixing in the separated shear layer. To date, researchers in the field of aerodynamics have applied these techniques through both experimental and numerical investigations. The following section provides a detailed explanation of these PFC techniques.

1.2.1.1 Vortex generators

Vortex generators, illustrated in Figure 1.7, are among the simplest and most effective PFC devices, widely used especially on wind turbine blades to prevent or reduce flow separation caused by adverse pressure gradients. Vortex generators are typically small rectangular or triangular plates installed on surfaces at specific angles to the flow [41]. Their primary function is to energize the slower boundary layer by mixing it with higher-momentum fluid from the outer boundary layer and freestream, which reduces drag and enhances lift.

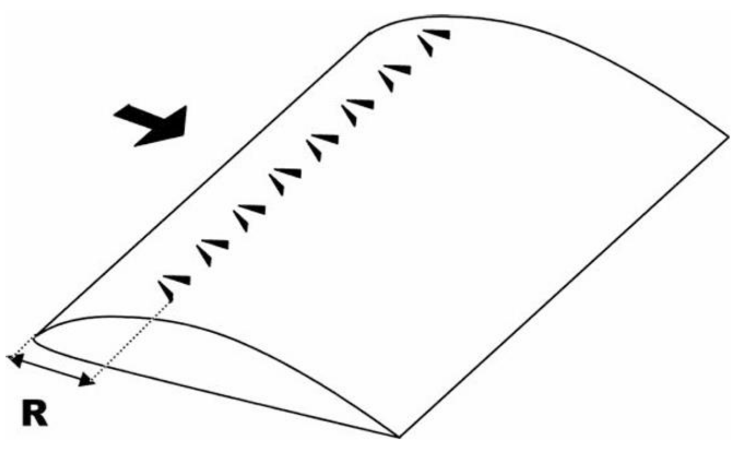

Figure 1.7. Vortex generators configuration [41]

To maximize their effectiveness, researchers have extensively studied vortex generator design parameters such as height, length, shape, spacing, arrangement, and mounting angle.

1.2.1.2 Leading-edge slats

Another PFC devices are Leading-edge slats which shown in Figure 1.8. The airflow between the slat and the main body is accelerated by the formation of either large vortices or several smaller vortices. Typically, large vortices form at lower Re, while higher Re produce smaller vortices. This acceleration imparts additional kinetic energy and momentum to the boundary layer, helping to delay stall onset [42].

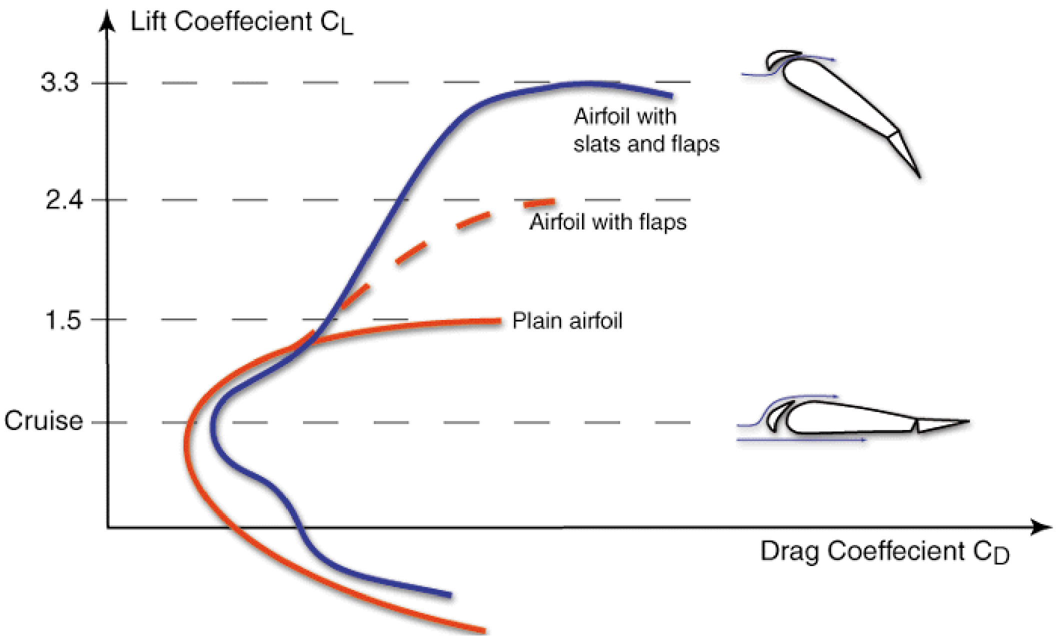

Figure 1.8. C_L comparison of slatted and unslatted wing [43]

1.2.1.3 Slotted airfoil

Slots, defined as narrow rectangular channels placed spanwise along a wind turbine blade, are a passive flow control technique used to modify airflow over an airfoil by increasing local flow velocity. As the internal airflow exits through the slot, its velocity rises, disturbing the surrounding streamlines and inducing controlled flow separation. This controlled separation slows down the flow over the airfoil, increasing the pressure on the lower surface and thereby generating additional lift. Slotted airfoil and slot characteristic shown in Figure 1.9.

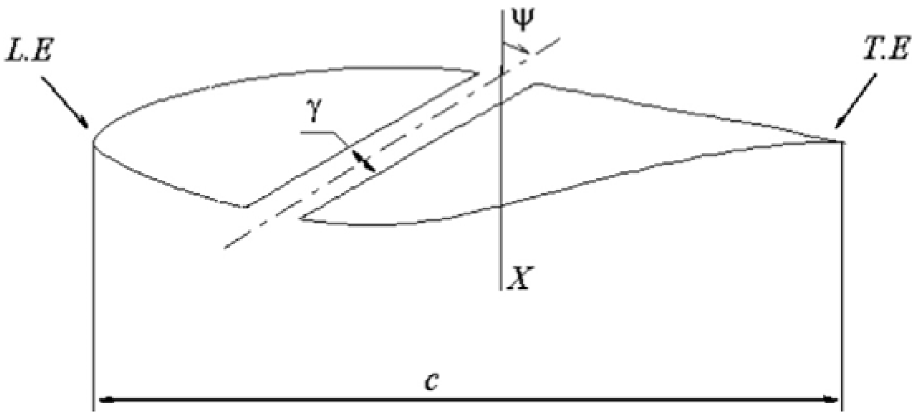

Figure 1.9. Slot geometric characteristics (c: Airfoil chord, LE: Leading edge, TE: Trailing edge, X: Slot location, Y: Slot width ψ: Angle between slot axis and chord normal) [44]

1.2.1.4 Gurney flaps

The Gurney flap, a small passive device attached to the TE of an airfoil, significantly enhances aerodynamic performance. This improvement is attributed to the formation of counter-rotating vortices downstream, which create a low-pressure region, increasing suction on the upper surface while raising pressure on the lower side [45].

Additionally combined applications, such as Gurney flaps with surface dimples, further improve aerodynamic performance, especially at higher angles of attack, as confirmed in numerical studies on symmetric NACA airfoils [46]. It can be seen the gurney flap effect on flow at high angle of attack in Figure 1.10.

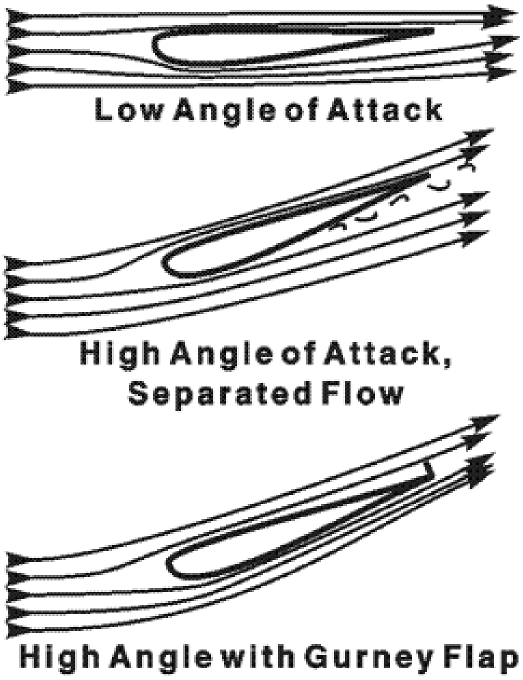

Figure 1.10. Effect of gurney flap [47]

1.2.1.5 Roughness material

Surface roughness as a PFC method can effectively improve aerodynamic performance of wind turbine blades, particularly at low Re. By introducing roughness elements such as sandpaper as shown in Figure 1.11, the boundary layer is energized through vortex generation, which aids in preventing separation caused by unfavorable pressure gradients, especially around the airfoil's leading edge (LE) [49]. This results in more stable and attached flow, similar to the effect of vortex generators [48].

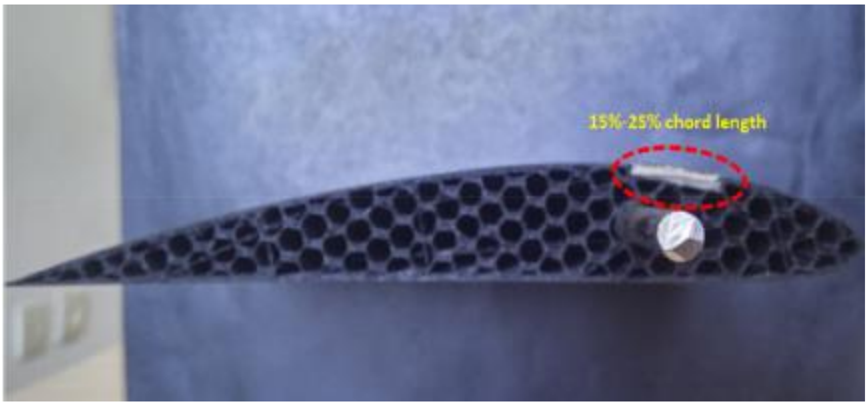

Figure 1.11. Sandpaper as roughness material on airfoil [49]

1.2.1.6 Flexible membrane wings

One of the important focuses in PFC research is the use of flexible membrane wings, particularly for improvement the aerodynamic performance of MAVs and UAVs. Inspired by biological flyers like bats, these wings feature a thin, compliant membrane attached to a fixed LE with a free TE as shown in Figure 1.12. This flexibility allows the wings to adapt to unsteady aerodynamic environments, making the flight of small aerial vehicles more stable and controllable. Additionally, flexible membranes help reduce structural weight while providing PFC benefits [50].

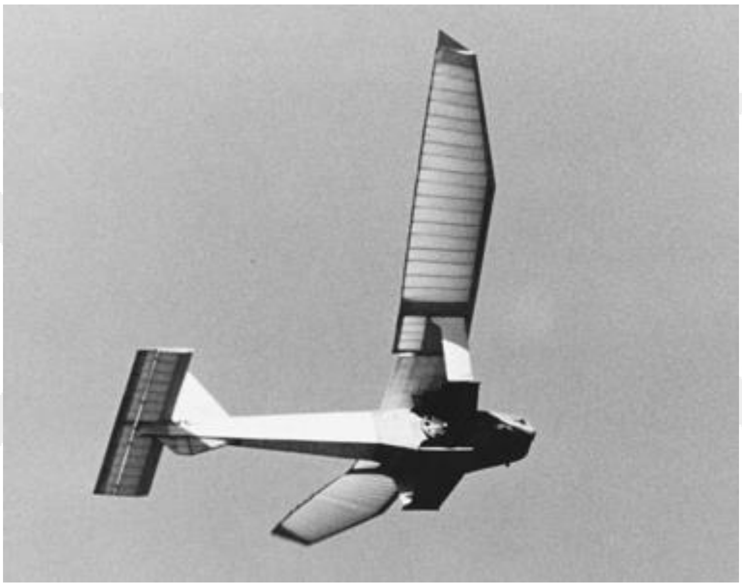

Figure 1.12. Flexible membrane applying on UAV [50]

Numerous experimental and numerical studies have explored the aerodynamic behavior of membrane wings, especially at low Re, where LSBs are more likely to form. Research shows that flexible wings can reduce the negative effects of LSBs, delay stall, and improve lift characteristics. Studies demonstrated generally that membrane wings at low aspect ratios undergo chordwise oscillations, particularly at high angles of attack [51]. Factors like excess membrane length and support geometry have significant effects on deformation, flow separation, and aerodynamic efficiency. Overall, studies consistently report that flexible membrane wings demonstrate higher lift-to-drag ratios, delayed stall, and improved aerodynamic efficiency compared to rigid wings.

1.2.1.7 Partially flexible airfoil

Using partially flexible membrane on the surface of airfoils is another PFC techniques on wing as shown in Figure 1.13. Even though comprehensive research on partially flexible membranes is limited in the literature, studies exhibit that flexible segments reduced flow separation, especially at high angles of attack, and increasing the lift coefficient near stall compared to the rigid airfoil [48].

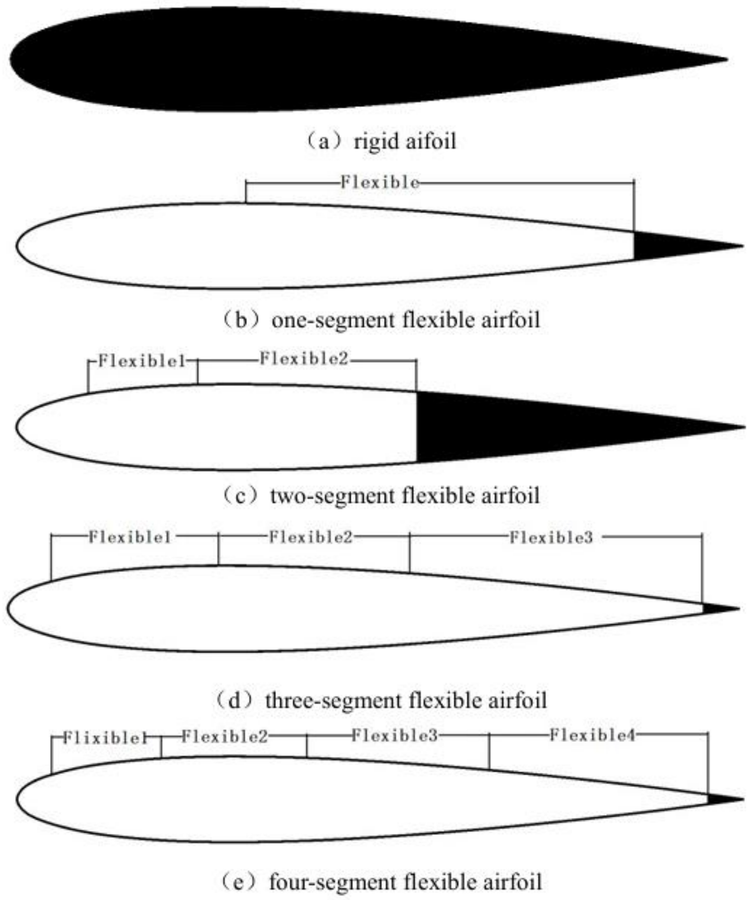

Figure 1.13. Partially flexible wing applying [52]

Beyond traditional approaches, it introduces an innovative concept of pre-stall control using surface roughness, full or partial flexibility supported by both experimental and numerical findings. PFC techniques can significantly enhance aerodynamic performance by effectively managing LSBs in the pre-stall phase. These novel pre-stall methods improve lift and reduce drag while requiring minimal material and energy input [53-56].

1.2.2 Active flow control

AFC technique, which is based on an external active intervention into the flow, requires energy as the main requirement. AFC techniques have been developed to achieve useful changes in the flow field, such as solving vortex shedding problems. There are two main advantages of AFC that cannot be achieved with passive techniques. First, AFC technology uses the inherent stability of the flow to achieve a large effect using small localized energy input and controls it. Second, AFC can be used to control complex, dynamic processes such as turbulence generation in turbulent boundary layers, thereby reducing skin friction and hence viscous drag, where the reduction is proportional to the surface area covered by the actuators [57]. The main advantage of AFC is that they can be applied or not applied depending on the changes in the flow conditions. On the other hand, the need the energy constantly that main disadvantage of the active control systems [58]. AFC techniques can be divided into groups as predetermined or interactive methods [59]. The predetermined method principle is based on the application of constant or non-constant energy without considering the state of the flow field. On the other hand, the principle of interactive methods is based on the continuous adjustment of the power input to the actuator depending on some kind of measuring element [60]. The following section provides a detailed explanation of these passive flow control techniques.

1.2.2.1 Plasma actuators

Plasma actuators are AFC devices that use ionized air to create a wall jet along a surface, adding momentum to the boundary layer. This helps delay flow separation, improve lift, reduce drag, and postpone stall, especially around leading-edge regions.

They work by applying high-voltage AC between electrodes separated by a dielectric, generating a body force on the airflow as shown in Figure 1.14 [61]. Plasma actuators are lightweight, fast, and require no moving parts, making them ideal for UAVs, MAVs, and wind turbines.

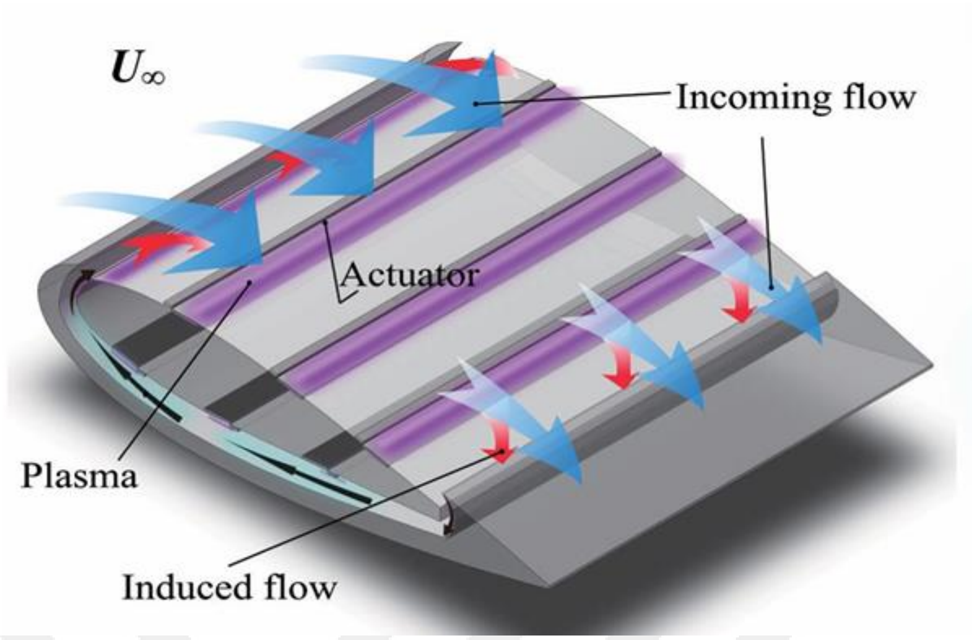

Figure 1.14. Plasma and actuator settlement on wing [61]

1.2.2.2 Synthetic jets

Synthetic jet actuators (SJAs) are active flow control devices that inject momentum into the boundary layer by periodically sucking in and expelling air through an orifice, without requiring external airflow [62]. An example of SJA shown in Figure 1.15.

Plasma-based SJAs (PSJAs) use spark discharges to generate high-speed pulsed jets, helping to delay flow separation, reduce drag, and improve lift. They use on suction surface to delay separation, especially at LE and separation points [63]. Additionally, there are examples on the flaps, slats or around the airfoil to direct flow. They are compact, have no moving parts, and operate at high frequencies, making them suitable for high-speed and high-Re flows.

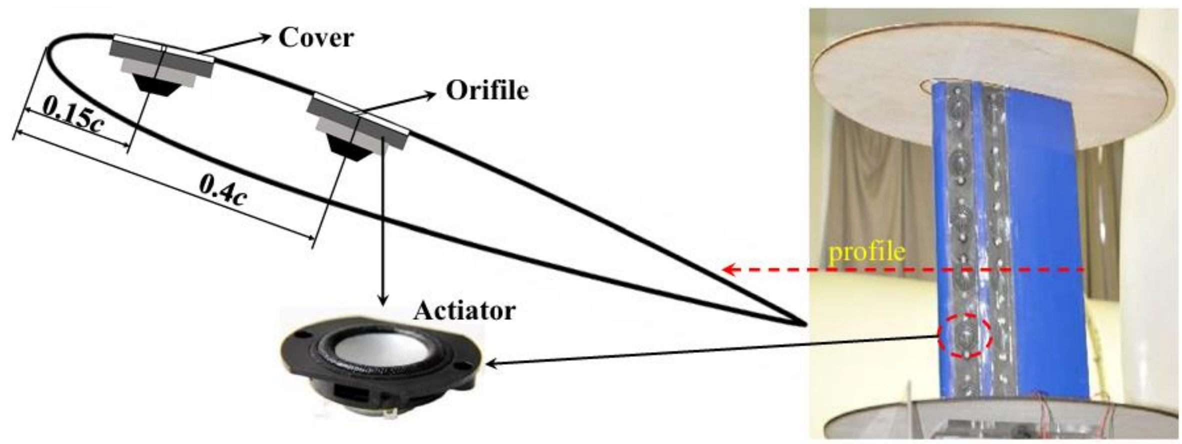

Figure 1.15. Apply of synthetic jet actuators on wing [63]

1.2.2.3 Magnetic fields

Magnetohydrodynamic (MHD) flow control utilizes the interaction between an applied magnetic field and an electric current within a conductive fluid to generate a Lorentz force (j × B) [64]. This force actively modifies the flow, particularly within the boundary layer, to delay separation and reduce drag. MHD techniques are mainly applicable to ionized flows and have potential use in aerospace systems for flow separation control and propulsion [65]. Advantages include no moving parts and direct flow manipulation. However, practical use is limited by high energy demands and the requirement for a conductive working medium.

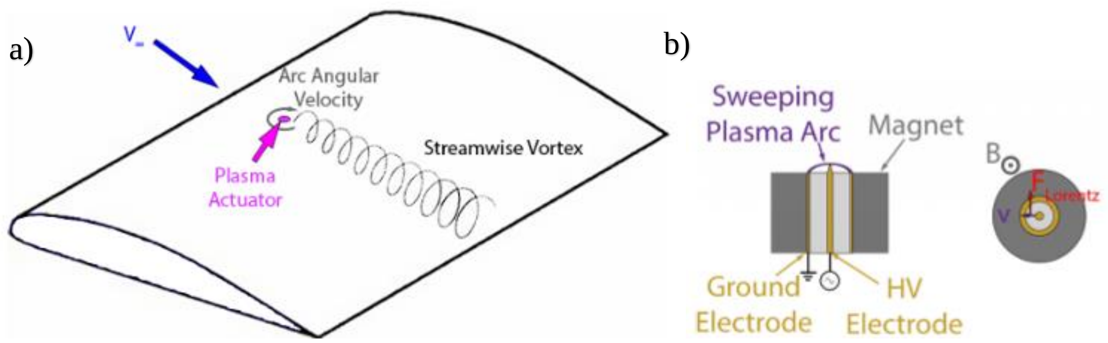

Figure 1.16. a) applying actuator on wing b) representative schematic of actuator [65]

1.2.2.4 Suction and blowing

Suction and blowing are active flow control techniques used to delay boundary layer separation and increase lift by adding or removing momentum near the surface of an airfoil. Blowing injects high-momentum air, energizing the boundary layer to prevent separation. Suction removes low-energy flow, stabilizing the flow and delaying stall [66]. Combined suction and blowing as shown in Figure 1.17 provide maximum lift-to-drag improvement, especially at high angles of attack [67].

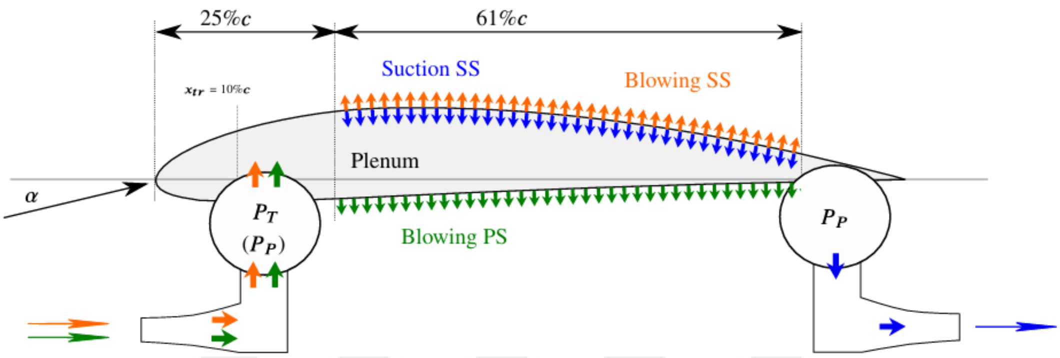

Figure 1.17. Control schemes, their locations, and schematic of components [67]

1.3. Motivation Of Study

The aim of this study is investigation of bubble characteristics and obtain the enhancement lift by using partial flexible surfaces on the wing at low Re. In addition to delaying the stall angle and reduce the drag coefficient by using partial flexible membrane on the wing. Revealing all these effects with oil and tuft flow visualization.

In this thesis study, the NACA 0018 wing type, which is widely used in wind turbines operating at low Re and UAVs cruising at low speeds and has also been the subject of many studies, was selected and flow events such as flow separations or laminar separation bubbles that negatively affect the aerodynamic performance on this wing profile were investigated in detail by experimental means. After detailed examination of these flow events, flexible membrane material was covered locally on the selected airfoil to minimize adverse flow events and increase aerodynamic performance. Experimental results of the passive flow-controlled airfoil and rigid airfoils (without flow control) covered locally with membrane will be shown comparatively in the following sections.

This thesis study consists of four main sections. In the first section, general information and literature review about the thesis study are presented. In addition, basic aerodynamic information is summarized. The section is concluded with a brief summary of the thesis.

In the second section, previous studies on flexible wings are mentioned and the results obtained from these studies are given.

The third section includes a general discussion of the experimental procedures. In this section, the experimental setup, equipment used and measurement techniques are explained in detail. The technical specifications and characterization of the wind tunnel are emphasized, and test equipment such as the manufactured wing, load cell system, balance and angle of attack plate and data acquisition software are discussed.

In the fourth section, the results obtained from the experimental studies are presented. All measurement data are analyzed with data processing and post-processing techniques. These data are meaningfully presented with graphs and tables. Error analyses in the measurements are also discussed to support data verification. The last section includes the summary, analysis and comparison of the measurement results with the outputs of the aerodynamic design tool.

2. LITERATURE REVIEW

2.1. Active Flow Control

2.1.1 Plasma actuators

Moreau et al. [61] examined the effect of a Plasma Co-Flow Jet configuration on NACA 0025 airfoil operating at a Re of 6.8 x 10^4. The results indicated a 31% delay in separation, supported by laser-based flow visualization and pressure measurements, confirming improved flow attachment and enhanced lift performance.

He et al. [68] performed a wind tunnel experiment on a NACA 0015 airfoil, implemented two spanwise arrays of weakly ionized plasma actuator at the LE and TE to mimic slat and flap effects. Results showed a 340% improvement in lift-to-drag ratio, increases in stall angle and maximum lift, achieved at only 2 W of power. The leading-edge array delayed separation via optimal unsteady actuation, while the trailing-edge array shifted the lift curve similar to a conventional flap.

In this study conducted by Moreau et al. [69] the use of DBD plasma actuators to control flow separation over a NACA 0015 airfoil was experimentally investigated. Three actuators were positioned individually along the upper surface of the airfoil at relative chordwise positions of x/c = 0.18, 0.27, and 0.37. The tests were performed at a Re of 3.3 x 10^6. Results showed that, without control, flow separation naturally occurred around x/c = 0.5. However, activating the DBD plasma actuator at x/c = 0.18 successfully postponed the separation point to x/c = 0.65. Furthermore, applying higher voltage extended this delay even further, pushing the separation location to approximately x/c = 0.76.

2.1.2 Synthetic jets

Zhao et al. [63] conducted wind-tunnel tests using SJAs on a NACA airfoil, revealing that jet inclination angle critically influences boundary-layer behavior and aerodynamic forces. They found that tangential jets, when actuated with high momentum, effectively delayed stall by energizing the inner boundary layer, whereas normal jets thickened the boundary layer and improved separation control at lower momentum levels.

Glezer [70] reviewed how surface-mounted synthetic jets interact with crossflow to actively control aerodynamic behavior; by generating discrete vortical structures, these jets transfer momentum without mass injection, enabling attachment control over stalled aero foils and bluff bodies. Applications presented include effective control of separation in both fully attached and separated flows, demonstrating the technique's versatility in enhancing aerodynamic performance.

De Giorgi et al. [71] performed numerical simulations comparing SJA and continuous jet actuators (CJA) for active flow control on both a NACA 0015 airfoil and a highly-loaded compressor stator cascade. They analyzed vortical structures, energy exchange, and momentum coefficients, finding SJAs consistently outperformed CJAs, offering about twice the reduction in total pressure losses under equivalent momentum input in the compressor cascade. The study demonstrated superior separation suppression and aerodynamic improvements with SJAs in both external and turbomachinery flows.

Lee et al. [72] designed a compact piezoelectric SJA and matched its forcing frequency to the natural stability frequency of a turbulent boundary layer, demonstrating efficient vortex generation with low power for flow control. Their study highlights the importance of actuator velocity output and resonance tuning to generate strong vortices and achieve effective synthetic-jet-based separation control.

2.1.3 Magnetic fields

Kral et al. [73] numerically investigated flow control using electromagnetic Lorentz forcing. Computational fluid dynamics (CFD) analyses were conducted on ship hull and channel flows to reduce separation and drag. Results showed that electromagnetic forcing improves flow stability and overall performance.

Donovan et al. [74] conducted both numerical simulations and experimental measurements to examine actuator behavior under various conditions. They investigated the performance of a Lorentz force actuator designed to control low speed airflow by generating body forces through electromagnetic interactions. Results demonstrated that the actuator could produce steady, controllable forces, making it suitable for boundary layer flow manipulation.

Zimmerman et al. [65] introduced the Cyclotronic Plasma Actuator, which generates a high-voltage plasma arc within a transverse magnetic field, inducing swirl via Lorentz forces. This on-demand vortex generator was experimentally and conceptually shown to delay boundary-layer separation without adding parasitic drag during cruise. The results underscore its viability for AFC, especially in aircraft takeoff and landing phases.

2.1.4 Suction and blowing

James et al. [75] conducted numerical simulations to examine the effect of secondary blowing in encouraging boundary layer separation and improving aerodynamic efficiency. They focused on NACA 0012 and LA203A airfoils within angle of attack ranges of 2° - 18° and 2° - 20°, respectively, using a jet positioned at x/c = 0.6. Findings indicated that the blowing technique delayed stall onset and contributed to an increase in lift coefficient.

Huang et al. [66] performed numerical analyses to investigate suction and blowing control strategies on a NACA 0012 airfoil at $Re=5 \times 10^5$ across multiple angles of attack. Their study focused on how variations in jet location, intensity, width, and direction affect the delay of flow separation and the modification of aerodynamic forces such as lift and drag. Results demonstrated that properly configured suction substantially enhances aerodynamic performance, increasing lift and reducing drag, while blowing shows limited benefit.

Fahland et al. [67] investigated turbulent boundary layer control over four-digit NACA airfoils using uniform blowing or suction. Control was applied to both suction and pressure sides across varying angles of attack, Re, airfoil camber, and thickness. Results exhibited that suction-side control confirmed prior results, while pressure-side blowing achieved up to 14% net drag reduction under optimal conditions.

2.2. Passive Flow Control

2.2.1 Roughness surfaces and grooves

Genc et al. [49] examined the effect of roughness elements as sandpaper experimentally and numerically on a NACA 4412 airfoil. Flow visualization, hot-wire, and force measurements showed that roughness enhances boundary layer momentum, stabilizes the laminar separation bubble, and resists adverse pressure gradients. As a result, stall is delayed and lift increases while drag decreases. These findings suggest that simple passive roughness can significantly improve aerodynamic performance of wind turbine blades in pre-stall conditions.

Koca et al. [76] investigated the effect of partially roughness surface on NACA 4412 as passive flow control technique. They positioned the sand paper on 15% - 25% of chord. Experimental results which have Re number of 2.5×10^4 - 7.5×10^4 showed that roughness surface is benefit for decreasing size of LSB in low Re flows.

Genc et al. [77] examined the effects of roughness element on airfoil. Sandpaper used as a roughness material in this experimental study. They worked in 2.5×10^4 to 1×10^5 Re number and it is chosen 15% and 25% chord distance on airfoil as a position of roughness element. Surface roughness enhanced the momentum within the airfoil's boundary layer, enabling the flow to better withstand the effects of adverse pressure gradients. Using sandpaper as a roughness material on airfoil suppressed the bubble and increased the C_L also decreased the C_D.

Mu et al. [78] implemented grooves as passive flow control method on the propellers of axial hydraulic pump and the results showed that grooves have significantly benefits on eliminating unstable region completely and they achieved the increasing performance of pump by ratio of 85%.

Seo and Hong [79] examined the effects of grooves on wind blade in this research. They obtained performance improvement with grooves. While lift to drag ratio improved by each Re which 2.8×10^5, 3.6×10^5, 4.5×10^5, and 5.3×10^5, it seen that the best condition increased the lift to drag ratio, at 15.3% in 3.6×10^5 Re number.

2.2.2 Gurney flap

Storms and Jang [80] analyzed surface pressure distributions and wake characteristics of a NACA 4412 airfoil to evaluate lift, drag, and pitching moment coefficients under various configurations. The integration of a Gurney flap elevated the maximum lift coefficient and reduced drag under near-maximum lift conditions. However, it also caused a drag penalty at low to moderate lift coefficients. Furthermore, the use of vortex generators on the baseline airfoil effectively delayed boundary layer separation, resulting in an overall increase in the maximum lift coefficient.

Yee et al. [81] conducted a numerical investigation into the aerodynamic behavior of Gurney flaps on NACA 0012 airfoils for rotorcraft applications, analyzing Mach numbers ranging from 0.2 to 0.9. Their study examined flap heights of h/c = 0.005, 0.01, 0.02, and 0.04, comparing the aerodynamic characteristics of modified and clean airfoils under static conditions. The results indicated that a flap height of h/c = 0.02 provided the most favorable aerodynamic performance, making it the optimal configuration for rotorcraft use.

Chandrasekhara [82] investigated the effect of adding a Gurney flap to VR-12 airfoil. Wind tunnel experiments showed that a 1% chord Gurney flap effectively restored the lift lost due to variable droop LE implementation while maintaining reduced drag and pitching moment. Lift-to-drag ratios improved, and dynamic stall onset was delayed, especially at Mach 0.3–0.4. Surface vorticity analysis confirmed that the Gurney flap enhances aerodynamic performance by mitigating adverse pressure gradients.

2.2.3 Leading edge slat

Wang et al. [42] numerically investigated the impact of leading-edge slats on the aerodynamic performance of the S809 airfoil and Phase VI wind turbine blade. Using the transition SST turbulence model, various slat geometries and positions were analyzed. Results show that appropriately placed slats significantly increase lift (up to 53%) and delay flow separation by shifting the separation point downstream.

Genc et al. [83] studied on NACA 2415 airfoil wing with the NACA 22 leading-edge slat in both experimentally and numerically. The results show that the stall angle delayed from 6° to 12° and obtained that 50% increase in the maximum lift coefficient.

Schramm et al. [84] examined numerically and optimized a leading-edge slat placed upstream of a DU 91-W2-250 airfoil using a gradient-based adjoint method. The optimized slat geometry resulted in a 2% drag reduction and slightly improved stall characteristics. The improvements remained effective even at higher Re, demonstrating robustness for wind turbine applications.

Mishra and Baeder [85] conducted a numerical analysis on the impact of leading-edge slats on rotor performance at a free-stream Mach number of 0.157 and a tip Mach number of 0.665. Using the SC2110 as the primary airfoil, they evaluated two slat configurations, S-1 and S-6. Their results showed that the S-6 slat enhanced thrust by approximately 10%, while both slat types significantly improved rotor performance even under demanding flight conditions.

Mendoza et al. [86] experimentally investigated the noise generated by a LE slat on a 2D wing model. Using an array of microphones small aperture directional array and pressure sensors, the researchers analyzed slat noise spectra, directivity, and scaling behavior. Results showed that slat noise is a distributed source, with high-frequency broadband components increasing with slat angle and gap velocity. The study also found that reducing the slat gap significantly decreases noise without severely affecting aerodynamic characteristics

2.2.4 Vortex generator

Delnero et al. [41] examined experimentally the aerodynamic effects of triangular vortex generators on a modified Eppler 387 airfoil at Re = 3 x 10^5. Vortex generators were placed at 10% and 20% chord positions with various incidence angles (0°, 10°, 20°). Results showed that maximum lift coefficient ($C_{L,max}$) increased up to 20%, while stall angle remained nearly unchanged. The findings confirmed that vortex generators enhance circulation and delay separation by energizing the boundary layer, especially at higher angles of attack.

Durhasan [10] examined the effect of single rod on SD7062 airfoil type in 3 x 10^4 Re number flow. The suction surface of the airfoil was equipped with a rod placed at different chordwise locations. Results showed that the how existing LSB forms on a standard airfoil and how placing a rod affects it. He found that positioning the rod correctly with the right diameter ratio could shrink the boundary layer height by up to 22%. Additionally, the rod significantly reduced unsteady vortices on the airfoil's suction surface, which in turn lowered turbulence intensity by as much as 30%.

Mueller et al. [87] used vortex generators for the application in wind turbines. Wind tunnel tests analyzed the effects of vortex generators' size, chordwise position, and spanwise spacing on lift, drag, and stall behavior. Results showed that properly placed small vortex generators increased the stall angle by up to 12.5° and lift coefficient by 31%, with acceptable drag penalties. Simulations confirmed that vortex generators can enhance performance and recover losses due to blade surface roughness across various rotor sizes.

Kundu et al. [88] demonstrated the effect of vortex generators on increasing gliding ratio on S1210 airfoil. The results of this study which performed numerically show that attaching counter-rotating vortex generators near the TE of the foil can increase the lift coefficient by 17% and delay the stall angle from 10 to 12.

Wang and Zhang [89] investigated NREL S809 airfoil using vortex generator to determine the aerodynamic efficiency. It was observed that the boundary layer thickness was because of vortex generators. Additionally the stall angle is increased from 14^o to 18^o when the vortex generators are installed at the 10% chord positions.

2.2.5 Flexible membrane

In this study Piquee et al. [90] studied with elasto-flexible surface to demonstrate effects on aerodynamic of wing. They worked both numerically and experimentally and the results showed that at positive angles of attack, because of the camber of airfoil increases, enhancing its lifting capacity. Additionally, stall onset occurs at higher angles of attack, and instead of a sudden drop in lift, the decrease becomes more gradual.

Demir and Genc [91] examined the unsteady flow behavior around flexible membrane which is AR = 3 experimentally in 2.5×10^4 and 5×10^4 Re numbers. As the aspect ratio increases, the LSB becomes more prominent on membrane wings operating at low Re, leading to intensified membrane vibrations that vary with the angle of attack at which the LSB begins to influence the flow. As a result, the unsteady nature of the LSB in membrane wings causes complex and unstable deformations of the wing surface.

Rojratsirikul et al. [92] investigated to aerodynamic characteristics of two-dimensional flexible membrane experimentally. Membrane airfoils with excess length tend to display higher vibration modes, earlier vortex roll-up, and reduced flow separation regions. In contrast, membranes under pre-strain behave more like rigid airfoils. The observed vibration frequencies of the membranes indicate a potential interaction with wake instabilities. The trend of Strouhal number reduces with the increase of angle of attack.

Genc et al. [93] investigated experimentally on flexible wing with different aspect ratio as AR = 1 and AR = 3 to demonstrate the tip vortex effect at 2.5×10^4 and 5×10^4 Re numbers. Experiment results exhibited that the high aspect ratio wings, leading-edge separation bubbles were found to significantly influence their behavior at low Re. In contrast, low aspect ratio wings, both tip vortices and leading-edge separation bubbles played a role in shaping their deformations.

Guo et al. [94] conducted wind tunnel testing using a simplified aircraft model to investigate how wing flexibility influences aerodynamic performance. In the best scenario, stall is delayed by nearly 5°, and lift increases by approximately 90% compared to the rigid wing model. This improvement is related to greater deformation and stronger vibrations in the flexible wing, which enhance flow mixing near the surface. Consequently, leading-edge separation is suppressed, leading to a remarkable boost in aerodynamic performance.

DeLuca and Reader [95] produced a micro air vehicle which has 60 cm, 15 cm span and chord of wing respectively to examine effect of wing flexibility on aerodynamic of MAV. They attached parachute material to wing and investigated the behavior of wing in wind tunnel experimentally. The findings showed that greater wing flexibility postponed stall onset and enhanced the peak lift-to-drag ratio by roughly 20% to 30% within a Re number range of 8.55 x 10^4 to 2.23 x 10^5.

Maqsood et al. [96] experimentally examined flexible wings for MAV applications at low Re number. Analysis of the wing skeleton revealed that all flexible wing configurations produced greater lift compared to the rigid wing. Among them, the configuration without battens generated the highest lift. In the membrane relaxation investigation, introducing relaxation caused to reduce lift and increase skin-friction drag. Furthermore, as the membrane extension increased, the lift generation consistently declined.

Laitone [97] performed a test rectangular planform wing at below Re 2 x 10^4 in a low turbulence wind tunnel. Across all Re below 7 x 10^4, the most effective configuration was having 5% circular arc camber compared base model. This profile consistently achieved the highest lift-to-drag ratio and the greatest lift coefficient at all angles of attack, regardless of turbulence intensity.

Akkala et al. [98] examined the kinematic and aerodynamic characteristics of sinusoidally plunging flexible airfoils inspired by biological and biomimetic flapping flight at 8.5 x 10^3 and 10 x 10^3 Re number. Comparisons with a rigid airfoil were conducted to evaluate the influence of structural deformation on vorticity evolution. As anticipated, the flexible airfoils generated higher thrust coefficients, while exhibiting lower lift and power coefficients than the rigid counterpart, resulting in substantially improved propulsive efficiency under all tested conditions.

Rojratsirikul et al. [99] performed an experimental study to investigate the unsteady aerodynamics of low aspect ratio membrane wings types as rectangular and delta in 2.4 x 10^4 to 5.9 x 10^4 Re range. Forces generated by membrane wings were measured and compared to those produced by rigid wings with similar shapes. The results showed that flexibility had a more pronounced positive effect on rectangular wings than on delta wings, leading to greater increases in both the maximum normal force and the force slope. Compared to rigid wings of equivalent shape, rectangular wings benefit more from flexibility, exhibiting a larger increase in both the peak normal force and the slope of the normal force. This enhancement is believed to result in the post stall regime from the membrane's responsiveness to wake induced vortex shedding.

Timpe et al. [100] investigated the response of flexible membrane on aerodynamic characteristic of simple flat plate wings. It is performed that a comparison of a rigid flat-plate wing and free trailing-edge membrane wings at Re = 5 x 10^4. Utilized the silicon rubber material as membrane with a scalloped free TE. The experimental data showed that flexible wings produced enhanced lift-curve gradients and sustained higher lift levels in the post-stall regime for angles of attack above 8°, resulting in overall aerodynamic performance gains, including in the pre-stall range.

Claever et al. [101] experimentally investigated wing flexibility for lift enhancement at 1 x 10^4 Re as well as the effect of wing oscillations. An experimental study was conducted to assess the aerodynamic, structural, and flow responses of rigid and flexible wings, spanning low to high aspect ratios, while oscillating at a constant 15° post-stall angle of attack and a chordwise amplitude of 15%. Results indicated that wing flexibility markedly enhances lift generation. Obtained that enhancement of C_L from 0.89 to 2.77 for low aspect ratio (AR = 3) and increased the C_L 1.04 to 3.14 for high aspect ratio (AR = 6).

Gordnier and Attar [102] numerically conducted flexible material on a membrane wing to observe the aerodynamic characteristics. Computations were performed at α = 10°, 16° and 23° for three different wings having two membrane flexibility at Re = 24.3 x 10^3. According to computation results, because of the flow control elements, it was observed that enhanced lift and reduced separation.

Greenhalgh et al. [103] performed inextensible flexible airfoil to determine its aerodynamic properties experimentally. They used end plate to eliminate effect of tip vortex. Experiments are done in two-dimensional wind tunnel. On the leading and trailing edges, the lift, drag and membrane tension force measured at the elliptical rods. Results of experiment exhibited that lift to drag ratio enhancement obtained at near the zero angle of attack.

Hu et al. [104] demonstrated an experimental investigation to highlight the aerodynamic advantages of flapping flight over fixed-wing configurations within a Reynolds number range of 1 x 10^4 to 1 x 10^5. The study compared the aerodynamic performance of two flexible membrane wings – one made from moderately flexible nylon and the other from highly flexible latex – with that of a traditional rigid wing, aiming to assess the influence of skin flexibility in flapping flight scenarios. The results demonstrated that the flexible wings offered superior overall aerodynamic efficiency (in terms of lift to drag ratio) compared to the rigid wing, particularly during high-speed soaring or at elevated angles of attack. Furthermore, the highly flexible latex wing exhibited the greatest thrust generation capability during flapping motion. In contrast, while the nylon wing showed the most favorable aerodynamic performance in soaring conditions, it delivered the poorest performance in flapping flight applications.

Shyy et al. [105] examined the wings of insects, bats, and birds, noting their anisotropic structural characteristics, and conducted a computational study on the aerodynamics of plunging, pitching, and flexible wings at low Reynolds numbers. Their findings reveal that leading-edge vortices (LEVs) commonly form at Reynolds numbers around (10^4) or below, conditions typical of insect flight. For instance, in the case of the hawkmoth, which operates within a Re of 10^3 to 10^4, the interaction between LEV formation and flapping kinematics significantly enhances lift generation. Additionally, a pronounced spanwise pressure gradient helps delay stall, while axial flow in the spanwise direction contributes to the stabilization of the LEV. It is observed that a membrane wing can enable passive shape adaptation by means of geometric or aerodynamic twist. Geometric twist improves streamlining, helping to reduce maneuver and gust loads while delaying stall by causing each wing section to rotate nose-down. In contrast, aerodynamic twist resulting from membrane inflation under load alters the zero-lift angle of attack, which enhances maximum lift coefficient, improves longitudinal static stability, and increases drag.

Li et al. [106] investigated the aeroelasticity of bio-inspired flexible membrane wings using three-dimensional (3D) variational fluid structure interaction solver at Re = 24.3×10^3, 36.5×10^3, and 48.7×10^3 numerically. A 3D rectangular membrane wing is then examined to analyze the 3D effect on the membrane aeroelasticity at 12.15×10^3, 24.3×10^3 and 48.6×10^3 Re numbers. Results exhibited the separated flow region of the flexible membrane wing is suppressed by the membrane flexibility, which results in the cambered-up shape thus achieving drag reduction and aerodynamic efficiency enhanced. The 2D flexible membrane wing obtained the aerodynamic efficiency gain of 52.16% at $\alpha = 8^\circ$, compared to its rigid counterpart. The lift-to-drag ratio of the 3D membrane wing was increased from 3.5 to 4.2 as the Re is quadrupled.

2.2.6 Partially flexible wing

Kang et al. [107] conducted an aerodynamic investigation on a partially flexible wing and demonstrated that the lift-to-drag ratio increased by over 80% at elevated angles of attack, with the stall angle shifting from 13° to 16°. Moreover, the incorporation of flexibility into the airfoil was found to diminish the size of the dominant vortex and reduce the shear layer thickness.

Another experimental investigation showed the implementing flexible membrane airfoils at low Re. In addition, the amount of riblets on a flexible wing was studied at Re = 7 x 10^4. The results demonstrated that using flexible membrane on airfoils offer superior aerodynamic efficiency when compared to rigid designs [108].

Acikel and Genc [109] aimed the controlling laminar separation bubble. Researchers covered NACA 4412 types airfoil with flexible membrane partially. The location of flexible surface cover determined by the according to results of experiments, yielding different locations scale with respect to the streamwise direction. They observed that partially flexible cover on wing delayed the stall angle and it produce enhancement of lift in 2.5 x 10^4, 5 x 10^4, 7.5 x 10^4 Re numbers. The best condition is obtained for the suppression of the LSB at Re = 2.5 x 10^4 with the partially flexible membrane, and the wake region of the airfoil cramped.

Genc et al. examined [110 displayed the influence of flexibility to enhance aerodynamic performance of wind turbines. Wind tunnel experiment was performed at 2.5 x 10^4, 5 x 10^4, 7.5 x 10^4 Re numbers. Results of experiment offered that the dimension of LSB constricted and increased $C_{L,max}$. However, the stall angle decreased in addition to the advantages of flexible surface.

Eroglu et al. [111] investigated the influence of partial flexibility on NACA 0018 airfoil experimentally in low-speed wind tunnel. Partial flexible cover on wing is significantly improved aerodynamic performance at Re = 3 x 10^4, and it also enhanced the lift coefficient and reduced the drag coefficient. The stall angle is delayed from 2.5° to 7°. However, the effect of flexible surface on the aerodynamic performance reduced with increasing Re. In addition, due to finite wing, the observed tip vortex influenced the LSB formation on surface of wing.

Mojtahedpoor and Naderi [112] studied numerically on NACA 0012 airfoil with local flexible to examine the unsteady flow separation on it. They chose the thermoset polyurethane as material of membrane and located at various locations. The best condition obtained at α = 8°

and 0 - 0.1 membrane location of chord length for the lift coefficient at 5 x 10^3 Re number. The stall angle increased from 10.5° to 12° as a result of the local flexible membrane. The findings indicate that incorporating a locally flexible membrane on the airfoil effectively suppresses flow separation, eliminates the formation of LSB, and contributes to stall delay.

Shyy et al. [113] numerically investigated effect of flexible membrane on S1223, NACA 0012, and CLARK-Y airfoil types at 7.5 x 10^4 to 2 x 10^6 Re number. To explore effective airfoil configurations for MAVs operating in unsteady low-Reynolds-number flows, XFOIL was adapted to model airfoils with membrane-covered upper surfaces. The flexible designs demonstrated enhanced stability in lift coefficient and more favorable lift-to-drag ratios when subjected to oscillatory freestreams, relative to rigid profiles.

Abudaram et al. [114] investigated the aerodynamic effects of elastic membrane wing which has 0.1 thickness intended for micro air vehicles experimentally at between 10^4 and 10^5 Re number. According the experiment results, wings equipped with thin battens help reduce flight loads by delaying stall and producing gentler lift curves. In contrast, thicker batten wings can increase flight loads due to effects like wash-in and cambering caused by membrane inflation, often generating very high lift values at elevated angles of attack.

Genc et al. [115] experimentally examined a flexible membrane wing with an aspect ratio of 1 at Re = 2.5 x 10^4 and 5 x 10^4. They utilized smoke wire technique for the flow visualization. The study revealed that low-aspect-ratio flexible membrane wings exhibit unsteady flow behavior characterized by tip vortices, vortex shedding, and their interaction. The findings showed that increasing the angle of attack led to greater membrane deformation. Additionally, as the angle of attack increased, the dominant vibration mode weakened, and the location of the maximum standard deviation moved closer to the trailing edge.

Hefeng et al. [116] investigated numerically four different cases where various regions of the wing were flexible. They examined aerodynamic effects by applying local flexible surface on wing at 1.35 x 10^5 Re number. The three-segment flexible airfoil demonstrated the highest performance among the four tested configurations, achieving a 39% increase in lift coefficient near the stall angle of attack when compared to its rigid version [80].

Lou et al. [117] numerical and experimental investigated on NACA 0012 by local vibration as flow control. The position of flexible skin is chosen at 0.065 – 0.09 of chord length from the

LE. The results of the study showed that local vibration triggered vortices in the shear layer near the short separation bubble, causing additional and smaller vortices to form. This resulted in a 23% reduction in the drag coefficient [81].

3. MATERIAL METHODS

3.1. Experimental Model

The experimental studies carried out in order to examine the effect of partial flexible surface on the aerodynamic characterisctic of NACA 0018 finite wing. The solid NACA 0018 symmetrical airfoil, which has c = 120 mm chord length and s = 480 mm span length, was chosen as the reference model. Schematic represantation of airfoil is presented in Figure 3.1. The partial flexible surface was created on the suction and pressure side of the airfoil, and it covers between x/c = 0.3 and x/c = 0.85 in the chordwise direction for all flexible surface wings (Figure 3.1b). On the other hand, the length of the flexible surface in the spanwise direction was changed with solid ribs to investigate the effect of the flexibility on the aerodynamic performance. In this context, the ribs will be produced from the airfoil section, and the ratio of rib thickness to wingspan will be selected as t/s = 0.0125 to create sufficient surface area for attaching the flexible material. One of the research parameters of the project subject was determined as the flexible surface ratio, sr/s (the ratio of the distance between the ribs to the wingspan), since the effectiveness of the flexible region on the aerodynamic coefficients will change depending on the distance between the ribs. (Figure 3.1c).

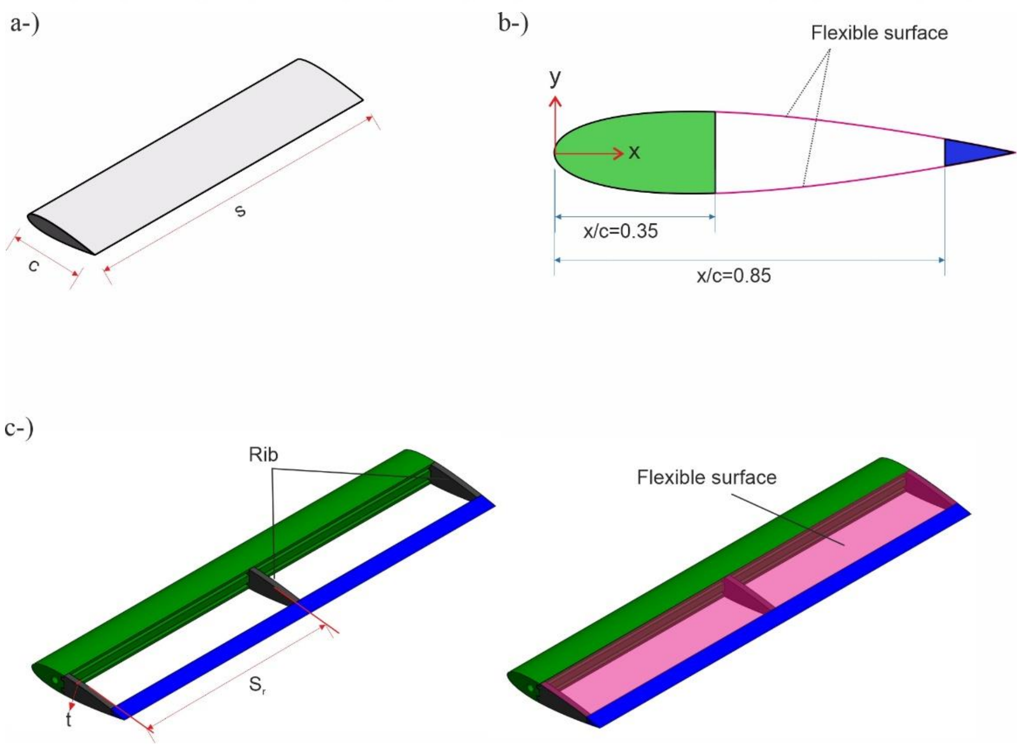

Figure 3.1. Schematic representation of test model

Four different flexible wings, which have Sr/s = 0.481, 0.234, 0.152, and 0.097, were examined in the present study. (Figure 3.2)

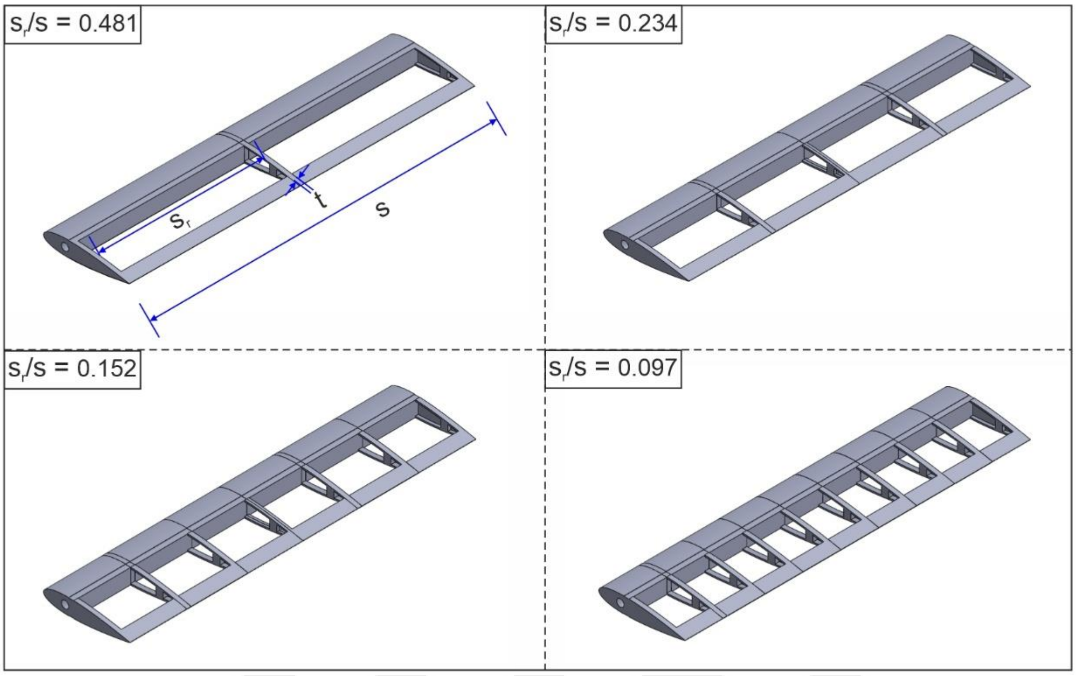

Figure 3.2. Schematic representation of wing models having partial flexible surface

All test models were designed using SolidWorks software and manufactured via 3D printer using PLA material. The flexible surface was created by covering the airfoil with a 0.2 mm latex rubber sheet, which has a Young's modulus (E) of 2.2 MPa and a density of 1 g/cm³ [92,118]. The manufacturing flowchart of the models is presented in Figure 3.3. In addition, images of the wing models with different flexible surface ratios are presented in Figure 3.4.

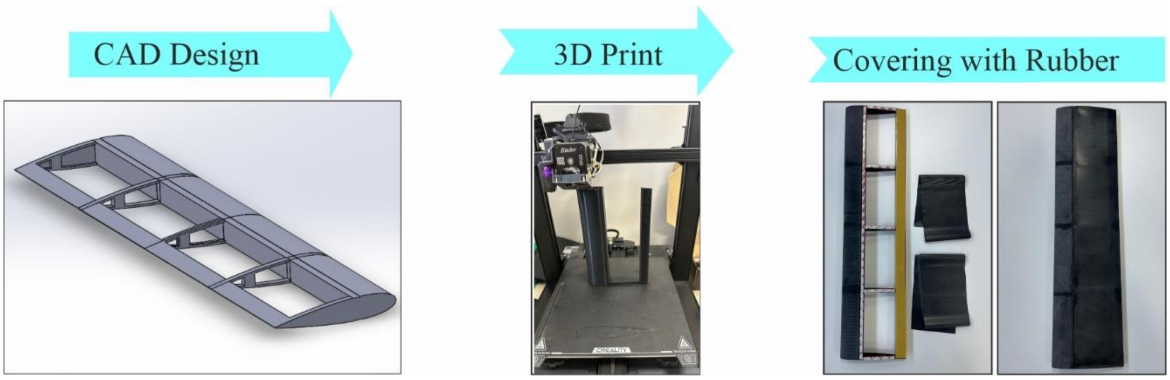

Figure 3.3. Flowchart of manufacturing the models

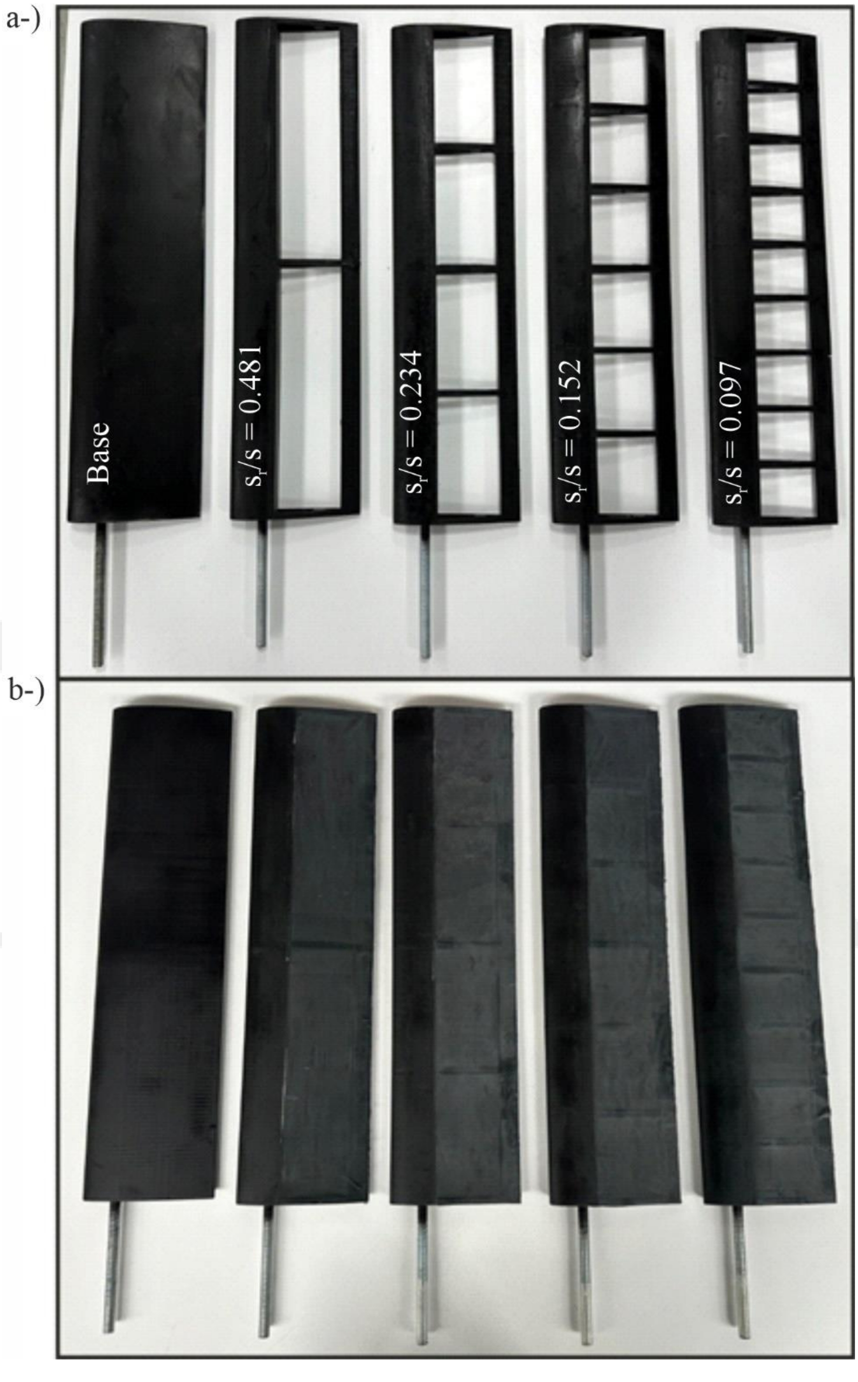

Figure 3.4. The wing models with different flexible surface ratios

3.2. Experimental setup and force measurement

All experiments were conducted in suction type, open circuit, subsonic wind tunnel in the Aerodynamic Laboratory of the Department of Aerospace Engineering in Adana Alparslan Turkes Scince and Technology. The components of the wind tunnel are the fan, diffuser, test section, and contraction (nozzle). To straighten the flow and lower the turbulence intensity by less than 1%, two fine mesh screens are positioned across the entrance. The contraction section has a ratio of 9:1. The wind tunnel (Figure 3.5a) test section which has of 600 x 600 x 1500 mm was constructed from a 20 mm thick transparent plexiglass sheet. Free stream velocity was controlled by a 15-kW axial fan with a variable speed control unit (Figure 3.5b). The free-stream velocity in the test section was determined using a Pitot-static tube with an electronic manometer (PCE HVAC-2) in order to adjust the free-stream velocity (Figure 3.5c).

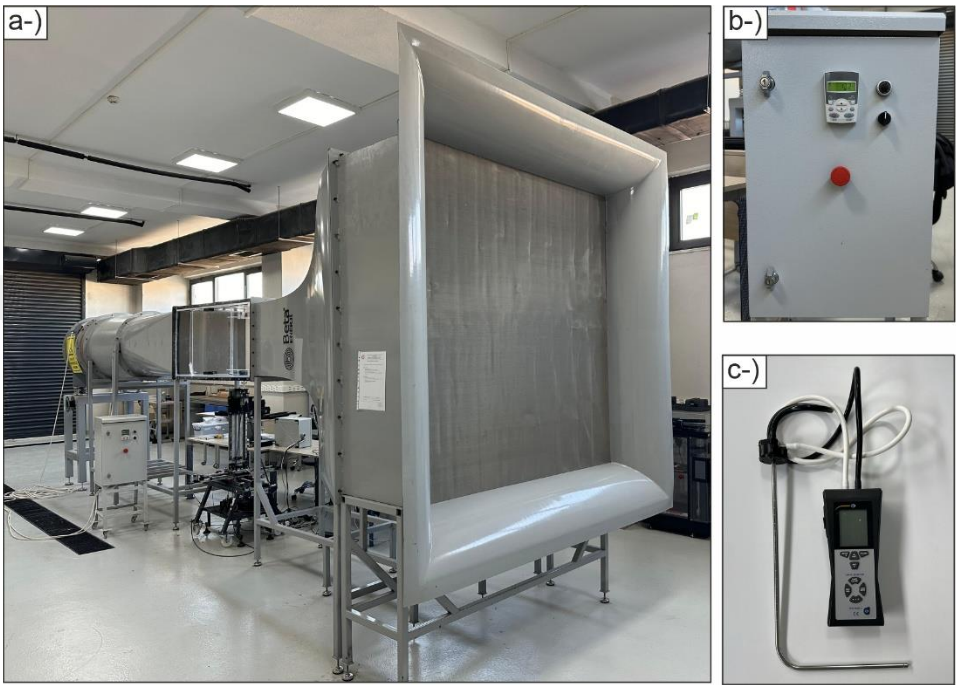

Figure 3.5. a) Open circuit, suction type subsonic wind tunnel, b) speed control unit, c) pitot-static tube with electronic manometer

In the experiments, the airfoil is positioned in the wind tunnel on the vertical axis via a three-axis traverse system. The traverse system moves in three axes, x, y, and z, and it gives the angle of attack to the test model via a servo motor. The servo motor is precisely adjusted using a rotating control unit. Positioning of the airfoil in the wind tunnel and the traverse system are shown in Figure 3.6. Force measurements were performed by using a six-axis force/torque (F/T) measurement system (ME-systeme-K6D40-50N-5Nm). The force/torque system consist of transducer, data acquisition (DAQ) card and GSV software with calibration data (Figure 3.6). The accuracy of transducer is about 2%.

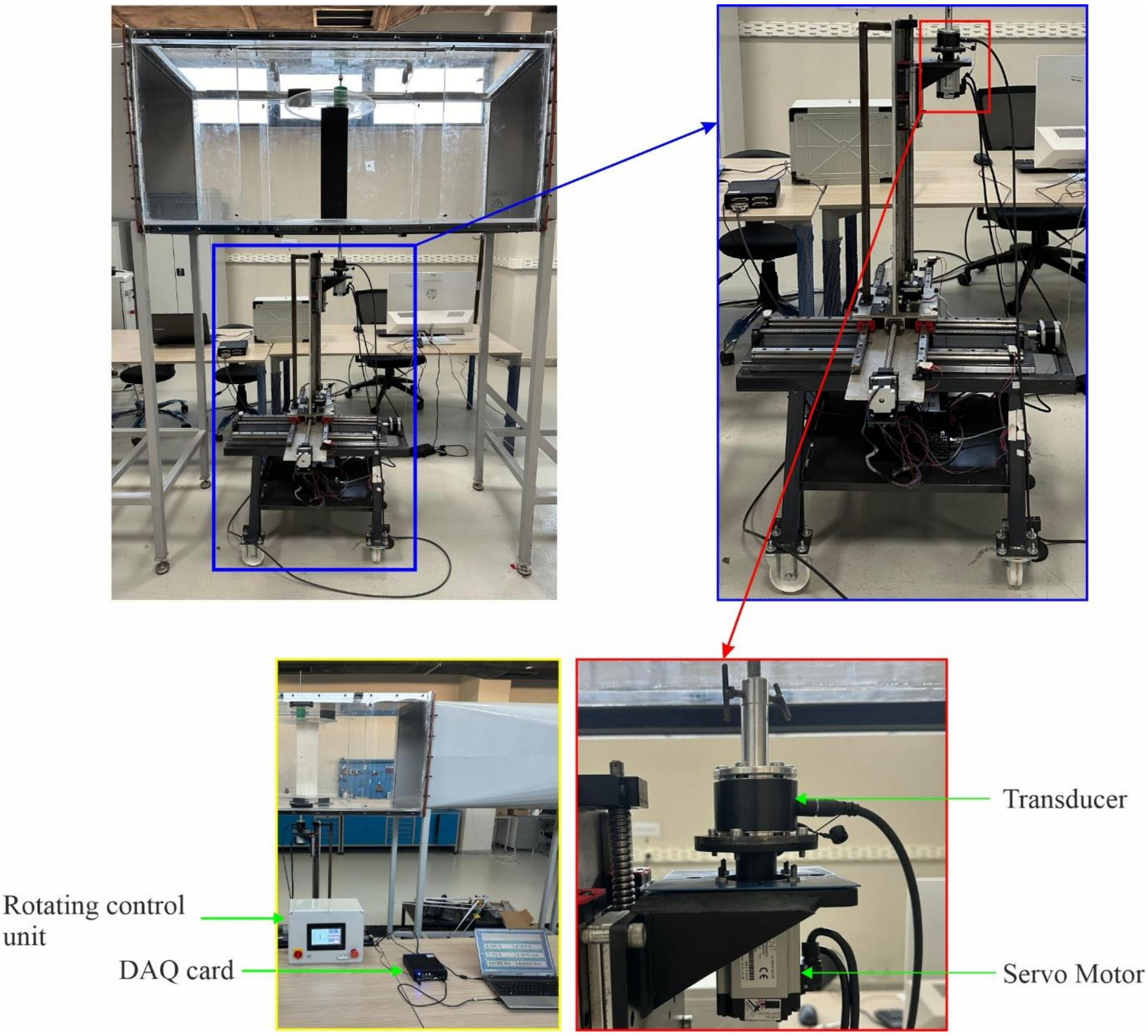

Figure 3.6. Positioning of the airfoil in the wind tunnel and the traverse system

To minimize the effects of the boundary layer, the endplate was positioned on the bottom surface of the wind tunnel, with a small gap. As Barlow et al. [119] mention, the gap between the model and the end plate was kept to a maximum of 0.5% of the wingspan length to avoid wall effect on the force measurements. Furthermore, to ensure the formation of tip vortices as observed in real flight conditions, a gap approximately equal to the chord length was adjusted between the tip of the wing and the tunnel wall. Karasu et al. [120] demonstrated that the distance between the wing tip and the wind tunnel being equal to the wing chord length is sufficient for the formation of tip vortices. A schematic representation of experimental setup is shown in Figure 3.7.

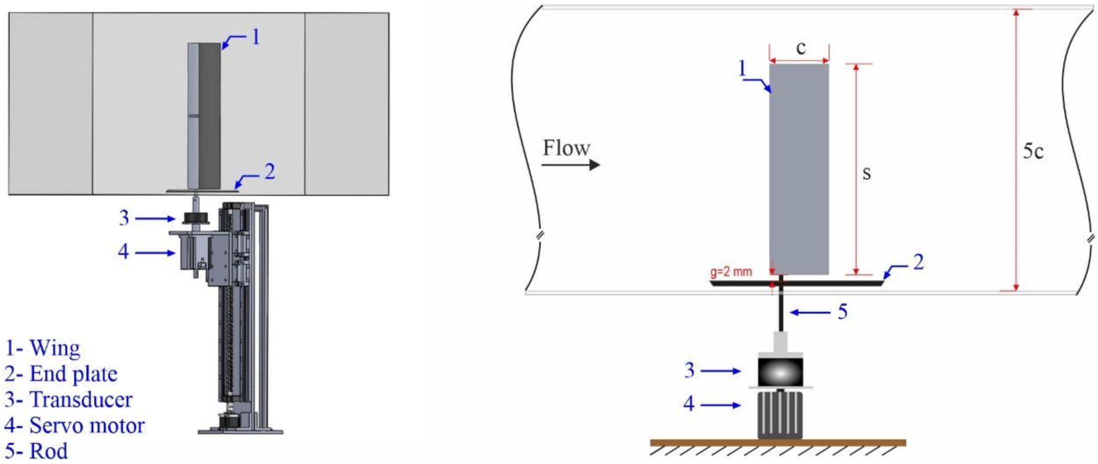

Figure 3.7. A schematic representation of experimental setup

Experiments were performed at four different Re as Re = 3 x 10^4, 5 x 10^4, 7 x 10^4, and 10 x 10^4 in order to investigate the effect of the Re on the aerodynamic coefficients of flexible wings. Re based on the chord length of the wing. Re calculated using Equation 3.1. The temperature of the Aerodynamic Laboratory was kept constant of 22° C throughout the experiments.

$$\mathrm{Re} = \frac{\rho U_\infty c}{\mu} \tag{3.1}$$

where ρ, U_∞, c, and μ denote the density of air, free-stream velocity, chord length of the wing, and dynamic viscosity of air, respectively.

Lift and drag force data were collected using six-axis load cell at a sampling rate of 1000 Hz over a time interval of 20 s for all cases. Force measurements were conducted at the angle of attack between $0° \leq \alpha \leq 18°$ with a 2° increment for all cases. In order to determine the stall angle precisely, force measurement experiments were carried out with an increase of 1° around the stall condition. After lift (F_L) and drag (F_D) forces were obtained, it has calculated the dimensionless coefficients of lift (C_L) and drag (C_D) in conjunction with Equations 3.2 and 3.3.

$$C_L = \frac{F_L}{0.5 \rho U_\infty^{\ 2} A} \tag{3.2}$$

$$C_D = \frac{F_D}{0.5 \rho U_\infty^{\ 2} A} \tag{3.3}$$

where ρ, U_∞, and A denote the density of air, free-stream velocity, and projection area of the wing.

3.3. Flow Visualization

Flow visualization has long been a foundational technique in experimental fluid mechanics, used to identify the position and scale of key flow features under investigation. Because most engineering fluids like air and water are transparent, visualization methods are necessary to make flow structures observable. In engineering practice, flow visualization is especially important for analyzing and optimizing flow behavior, particularly in complex, three-dimensional configurations. During testing, models were positioned horizontally to capture clearer images of the surface flow patterns. In order to explore the flow characteristics qualitatively over the wings, surface oil and tuft flow visualization experiments were performed in the present study. The angles of attack were determined based on the aerodynamic coefficient results.

3.3.1 Surface oil visualization

Surface oil flow visualization is a relatively straightforward yet widely utilized technique in wind tunnel testing, offering valuable insight into surface flow behavior. It involves applying a thin film of oil to the airfoil surface to capture flow features through photography. The method is cost-effective, easy to implement, and particularly useful for identifying flow topology and boundary layer development. The oil mixture must possess appropriate viscosity to accurately reveal separation lines, as the oil is unable to cross separation regions [121].

Commonly used oils for this technique include kerosene and transformer oils. In this study, 5W-30 a fully synthetic engine oil was selected, with titanium dioxide (TiO_2) powder as the pigment due to its white, opaque nature, which provides strong visual contrast against a matte black-painted airfoil surface. Oleic acid was used as the additive solver for TiO_2.

The mixture ratio TiO_2 powder, oleic acid, 5W-30 and, kerosene respectively oil in a 1:5:7:2 proportion was adapted. The oil was applied with a brush to both pressure and suction sides of the airfoil until uniformly coated. The wind tunnel remained operational until the oil dried, after which high-resolution images were taken using a GoPro HERO 11 camera (27 MP) to document the resulting flow patterns.

3.3.2 Tuft flow visualization

Tuft flow visualization is a simple yet effective technique widely used in wind tunnel experiments to qualitatively observe surface flow behavior. The method involves attaching small, lightweight yarn or thread tufts to the surface of the airfoil, which align with the local flow direction when exposed to moving air. This allows researchers to visually detect flow separation, reattachment, and turbulent or reversed flow regions in real time. Tuft visualization is especially valuable for low-speed aerodynamic testing due to its low cost, ease of setup, and ability to capture dynamic changes in flow patterns.

In this study, white nylon yarns approximately 20 mm in length and 0.2 mm in diameter were used as tufts. The tufts were attached in a grid pattern across the upper and lower surfaces of the airfoil using a small amount of adhesive. To enhance visual contrast during flow visualization, the airfoil was painted matte black. The wind tunnel was operated at various speeds and angles of attack, and tuft motion was recorded using a GoPro HERO 11 action camera (27 MP) positioned above the test section.

3.4. Validation Of Experiment

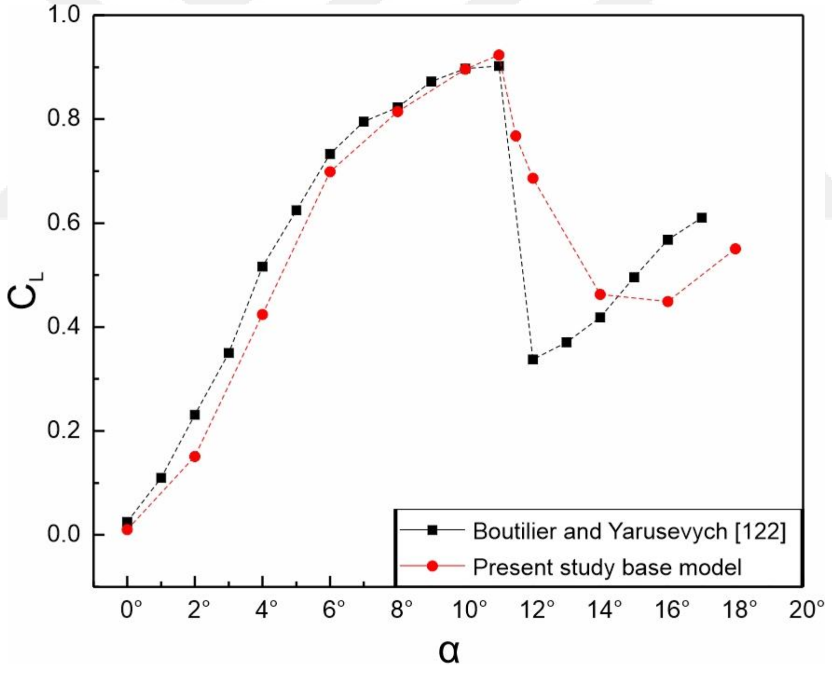

Figure 3.8. C_L versus alpha

It was determined that the lift coefficients of NACA 0018 base model which obtained from the experiments at Re = 10 x 10^4 were compatible with the study of Boutlilier and Yarusevych [122].

4. RESULTS AND DISCUSSIONS

In this section, the effect of flexible surface on the aerodynamic performance of the NACA 0018 airfoil is discussed in detail with force measurement and flow visualization techniques (surface oil flow and tuft). The obtained results are also compared the base wing (wing with solid surface).

In Figure 4.1, the variation of lift coefficient (C_L) with respect to angle of attacks is presented for all wings at Re = 3 x 10^4, 5 x 10^4, 7 x 10^4, and 10 x 10^4. Since the wing models have a symmetrical profile, the C_L value is obtained as zero at the angle of attack α = 0°. For the Re = 3 x 10^4 value, the stall angle of the wing model with solid surface is determined as α = 2,5° and its $C_{L,\ max}$ = 0.0873 before the stall (Figure 4.1a). The obtained this result is good agreement with the Rogowski et al. [123]. They conducted an experimental study in the wind tunnel in order to determine aerodynamic coefficients of NACA 0018 airfoil at low Re. They indicated that lift coefficient of NACA 0018 is practically negligible at Re = 3 x 10^4. On the other hand, it is clearly seen that the flexible surface is remarkably effective on the lift coefficient. It is observed that the C_L value increases with increasing angle of attack. For the wing model with flexible surface ratio Sr/s = 0.481 and Sr/s = 0.234 the maximum C_L angle of attack is obtained as α = 6° and C_L = 0.488 and C_L = 0.556 respectively. In other words, the stall angle is shifted by 3.5° compared to the wing model with solid surfaces, and the maximum C_L value is increased by 458% and 536%, respectively. On the other hand, it is observed that the effect of flexible surface on the C_L value decreases for Sr/s = 0.097 in comparison with other flexible surface ratios. However, Sr/s = 0.097 wing model produce remarkably lift force and it has certain stall angle when compared to the wing model with solid surfaces.

The variation of C_L at Re = 5 x 10^4 is shown in Figure 4.1b. It is observed that Re number is an effective parameter on the lift coefficients. For the wing model with solid surface, the maximum C_L values and the stall angle were determined as C_L = 0.673 and α = 7°, respectively at Re = 5 x 10^4. On the other hand, it is observed that the C_L values of the wing models with flexible surface are lower than the wing model with solid surface at Re = 5 x 10^4 in the range of 0° ≤ α < 6° of the attack angles (Figure 4.1b). However, it is observed that the stall angle was around α = 8° and the maximum C_L values are increased by 13% for flexible surface ratio of Sr/s = 0.481, 0.234, and 0.152 when compared to the base model (solid surface). Besides, the wing models with flexible surface are also effective for post stall angles and the C_L values are higher than the wing model with solid surface.

The results obtained at Re = 7 x 10^4 are presented in Figure 4.1c. It is clearly seen that the effect of the flexible surface on the lift coefficient decreases significantly with the increase of Re, especially before the stall angle. For the wing with solid surface at Re = 7 x 10^4, the stall angle and the value of the maximum C_L are determined as 10.5° and 0.876, respectively. It is observed that C_L of flexible surface is lower than that of a solid surface. However, the stall angle of the flexible surface is slightly changed when compared to the solid surface. On the other hand, C_L values of the flexible surface at post-stall angles are higher than the solid surface. A similar trend is also observed at Re = 10 x 10^4 (Figure 4.1d). Especially for high flexible surface ratios, C_L values are lower than the base wing model; however, they have high values at post-stall angles.

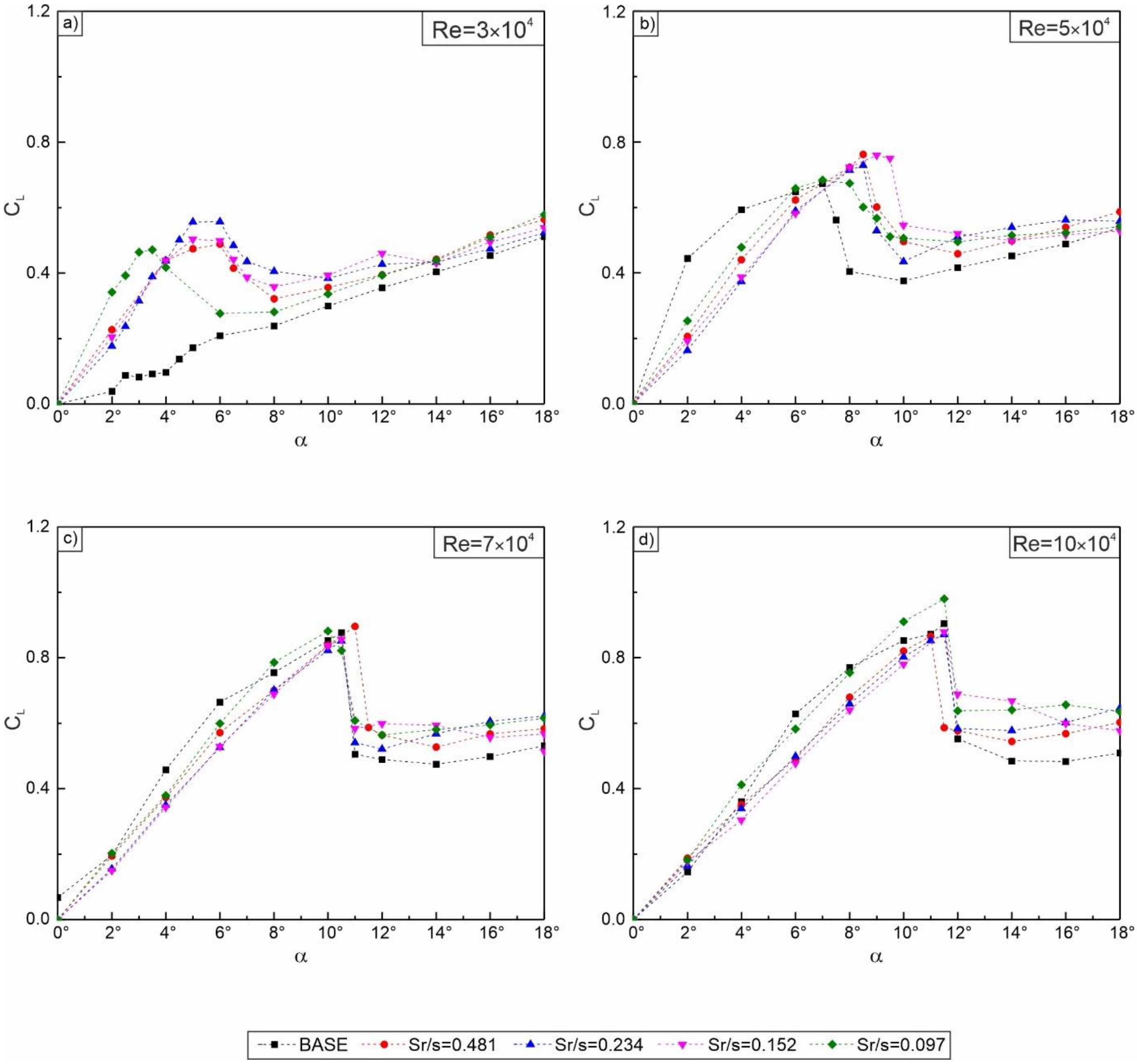

Figure 4.1. The variation of C_L with respect to angle of attack at different Re

Figure 4.2. shows the drag coefficient variations with the angle of attack for all wing models at different Re. The obtained results indicates that flexible surface are not only effective on the lift coefficient but also on the drag coefficient. It is observed that especially before the stall angle, the C_D values of the wing models having low flexible surface ratio decrease significantly when compared to the wing model with solid surfaces. The value of C_D increases with increasing angle of attack. A sharp increase in Cd indicates the formation of the stall on the wings, and the stall angle is postponed with the increasing Re. On the other hand, the flexible surface adversely affects the CD at post stall angles, especially for low Re. The values of C_D at post stall angles for wings with flexible surface are higher than the wing with solid surface. The

sudden increase in C_D (which occurs at approximately 11° and 12° angles of attack for Re = 7 x 10^4 and 10 x 10^4, respectively) indicates the stall condition.

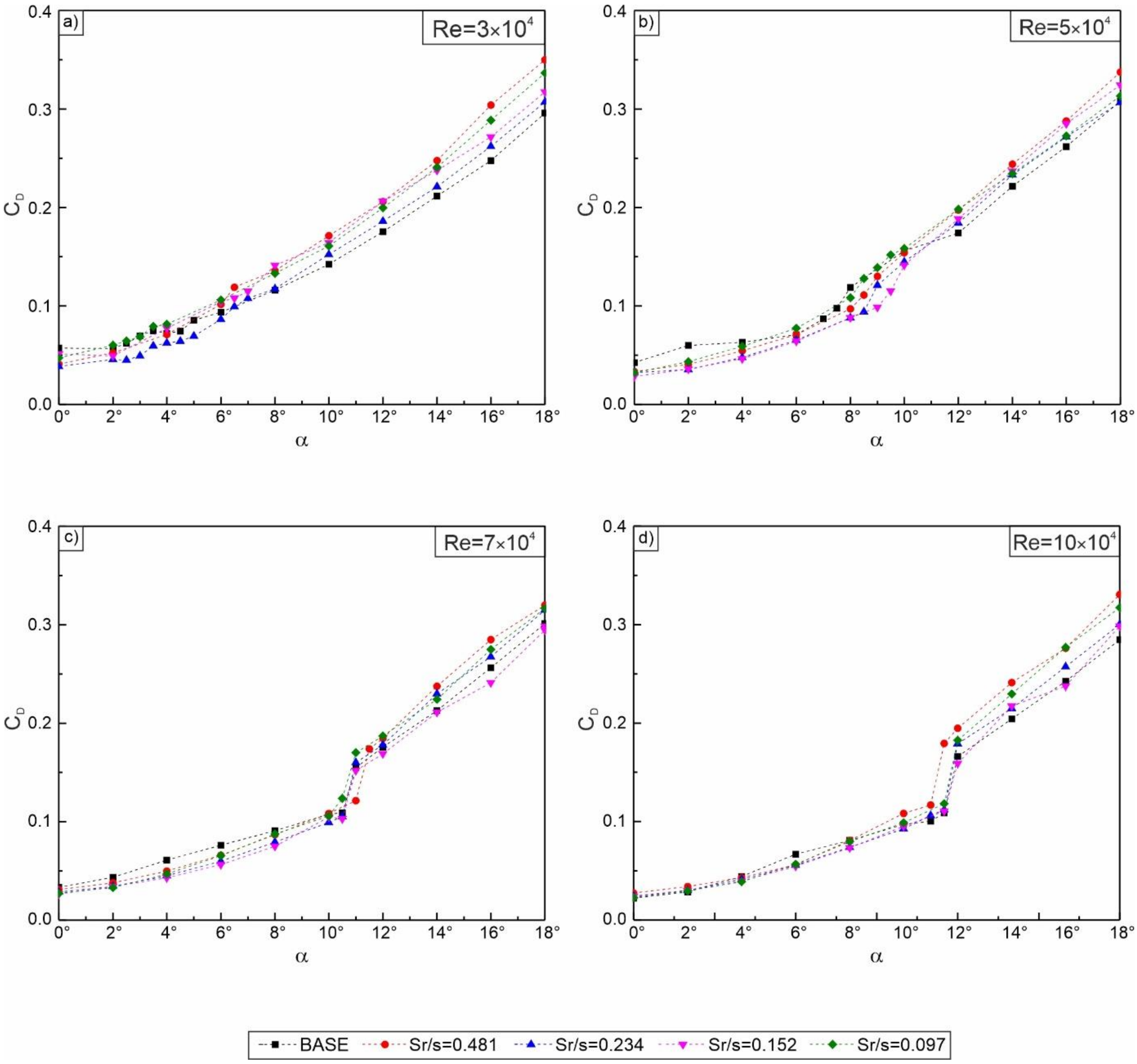

Figure 4.2. The drag coefficient variations with the angle of attack for all wing models at different Re

In order to investigate the effect of the flexible surface on the wing aerodynamic performance, the ratio of the lift coefficient to the drag coefficient (C_L/C_D) is also evaluated. Figure 4.3 shows the variation of C_L/C_D with respect to the angles of attack for all wing models at different Re. The flexible surface cause increase in lift force as well as reduction in drag force. Therefore C_L/C_D remarkably increased when compared to the solid surface. The maximum C_L/C_D is obtained for Sr/s = 0.234 at Re = 3 x 10^4 (Figure 4.3a). When compared to the solid surface, it increases by at least 425%. The aerodynamic performance of the wings with flexible surface decreases with the increasing Re. It is observed that the value of C_L/C_D of wings with flexible surface is lower than the base wing for pre-stall angles at Re = 5 x 10^4 (Figure 4.3a). However, it gets higher values for post stall angles. The variation of C_L/C_D with respect to angle of attack for all wing models at Re = 7 x 10^4 and 10x10^4 are presented in Figures 4.3c and 4.3d, respectively. It is observed that C_L/C_D values increase with increase angle of attack at Re = 7 x 10^4 and 10x10^4 for all wing models. The maximum C_L/C_D is reached at angle of attack in the range of 6° ≤ α ≤ 10°, and their magnitudes get close to each other. However, it is determined that the effective flexible surfaces ratio on maximum C_L/C_D is Sr/s = 0.152 and 0.481 at Re ≥ 7 x 10^4.

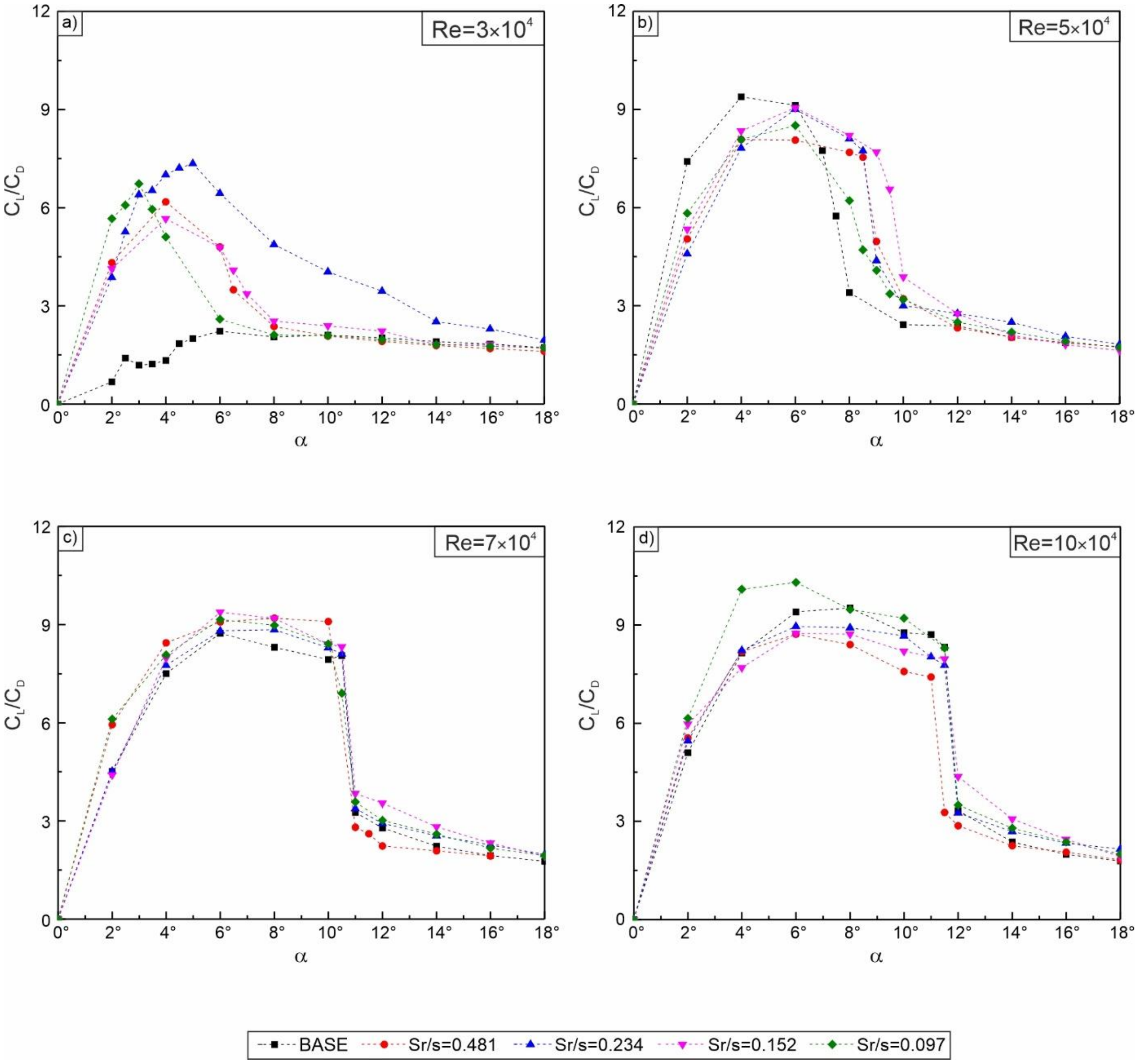

Figure 4.3. The variation of C_L/C_D with respect to angle of attack for all models at different Re

In order to reveal flow characteristics over the wing models, surface oil and tuft visualization experiments are performed for α = 4º, 8º and 12º at Re = 10 x 10^4. Figure 4.4 shows surface oil flow and tuft visualization of base model at α=4°. Surface oil visualization depicts that flow separates approximately at x/c=0.2 and then it reattaches nearly at x/c = 0.5 (Figure 4.4a). As a result of this phenomenon, a laminar separation bubble (LSB) occurs between x/c = 0.2 and 0.5. Furthermore, a tip vortex formation is seen at the free end of the finite wing. The tip vortex directs the flow inwards and creates a chaotic flow structure marked by the blue line in this figure. Moreover, it affects the LSB over the wing with solid surface. Figure 4.4b presents tuft visualization of base model at α = 4°. Although tuft visualization does not give information about LSB, it clearly depicts that the formation of the tip vortex directs the flow inwards.

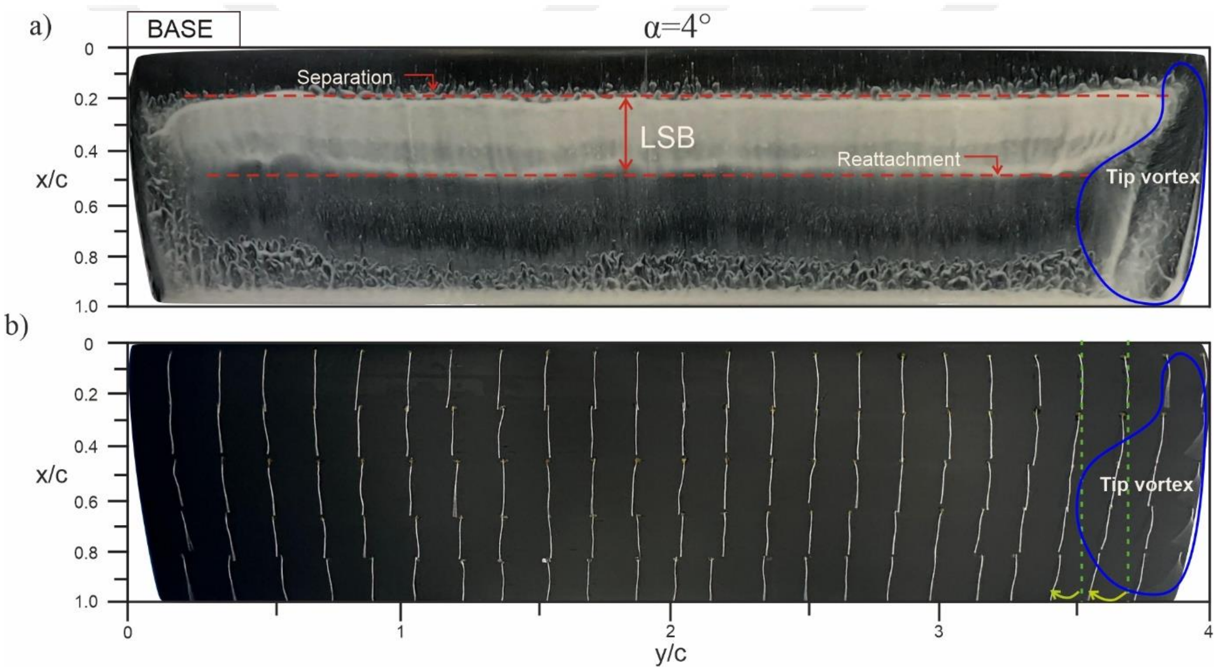

Figure 4.4. Surface oil and tuft visualization over the base model at α = 4°

Figure 4.5 illustrates the surface oil and tuft visualization for base wing at α = 8º. It is observed that the separation line gets close to the LE when the angle of attack increases from α=4° to 8°. The reattachment occurs nearly at x/c = 0.25. Therefore, the size of LSB also decreases with the increasing angle of attack. On the other hand, the surface oil and tuft visualization depict that the tip vortex affects the flow over the wing.

The visualizations obtained from surface oil and tuft experiments for base wing at α = 12º are presented in Figure 4.6. The results of both visualizations indicate the flow separates nearly LE and it does not reattach the wing surface. As a result of this phenomena stall occurs. In particular, the result obtained from the tuft experiment depicts that the stall causes an unsteady and chaotic flow over the wing. On the other hand, it is seen that tip vortex formation is also effective over the wing.

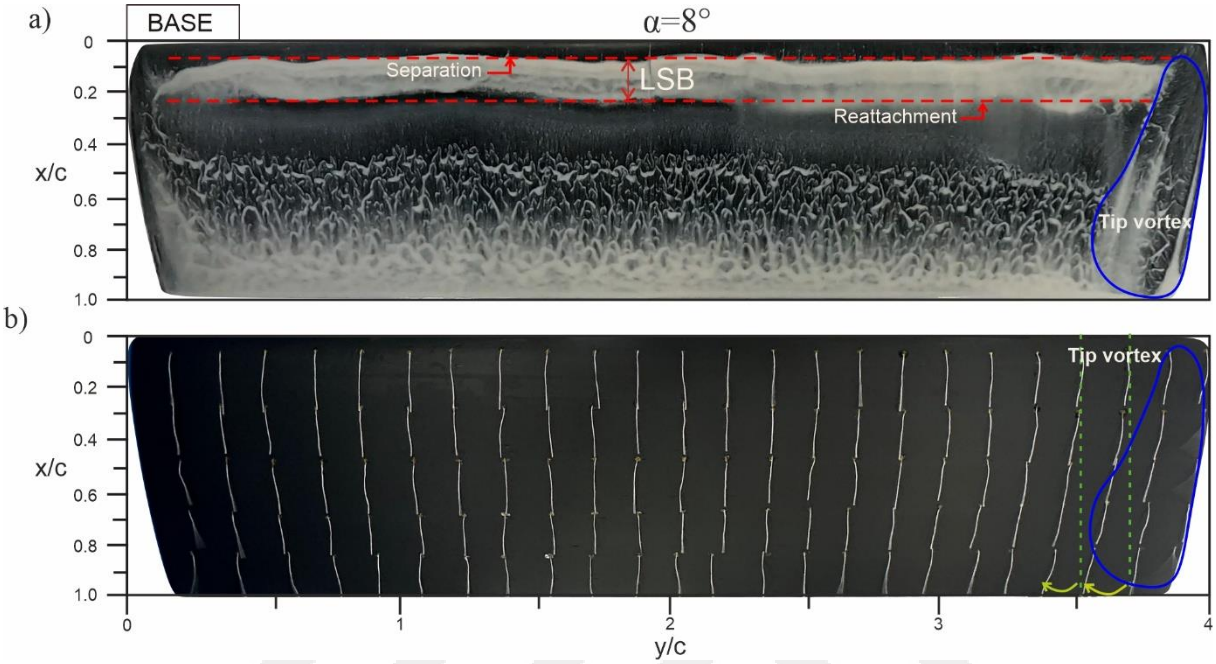

Figure 4.5. Surface oil and tuft visualization over the base model at α = 8°

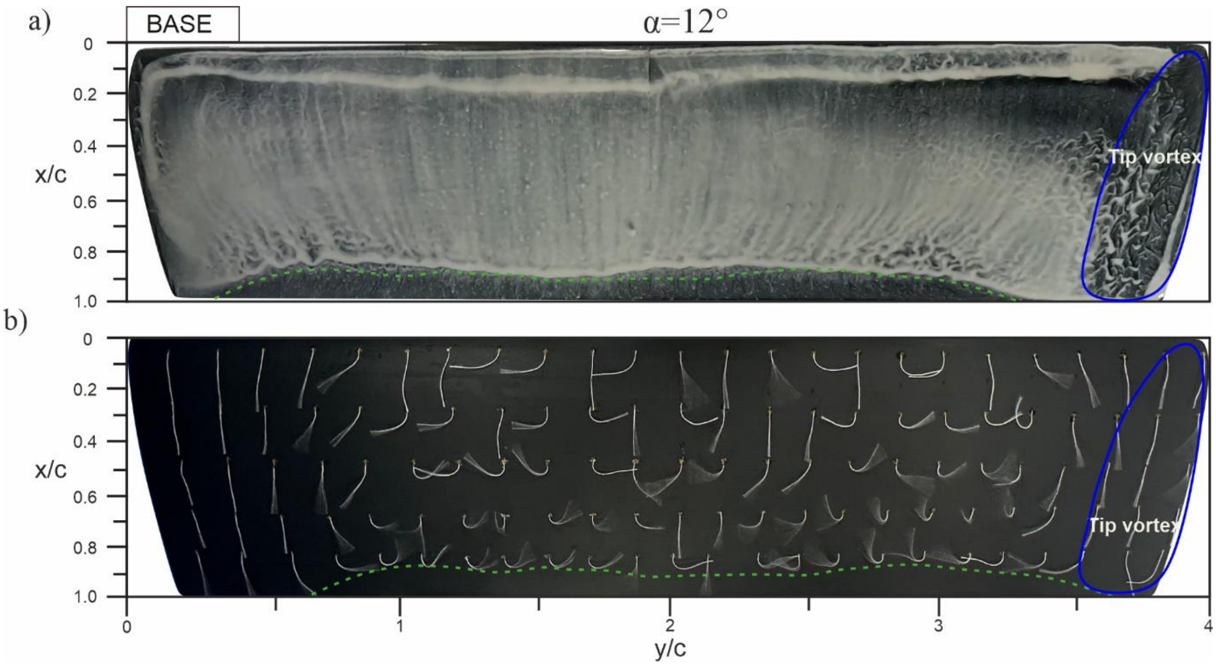

Figure 4.6. Surface oil and tuft visualization over the base model at α = 12°

Since the oil mixture used in surface oil visualization causes deformation of the latex rubber sheet, tuft visualization experiments were only performed for wings with flexible surfaces. Figure 4. 7 presents tuft visualization of Sr/s = 0.481 model at α = 4°, 8° and 12°. It is observed that tip vortex affects the flow over the wing at all angle of attacks. Furthermore, stall occurs at α = 12° for Sr/s = 0.481 model. Tuft visualization results obtained for Sr/s = 0.234, 0.152, and 0.097 at different angles of attack are presented in Figures 4.8, 4.9, and 4.10, respectively. It is observed that tip vortex affects flow over the wing for all wing models, and it causes the flow to direct inwards. Besides, stall is observed at α = 12°, and these results are in good agreement with the force measurement results.

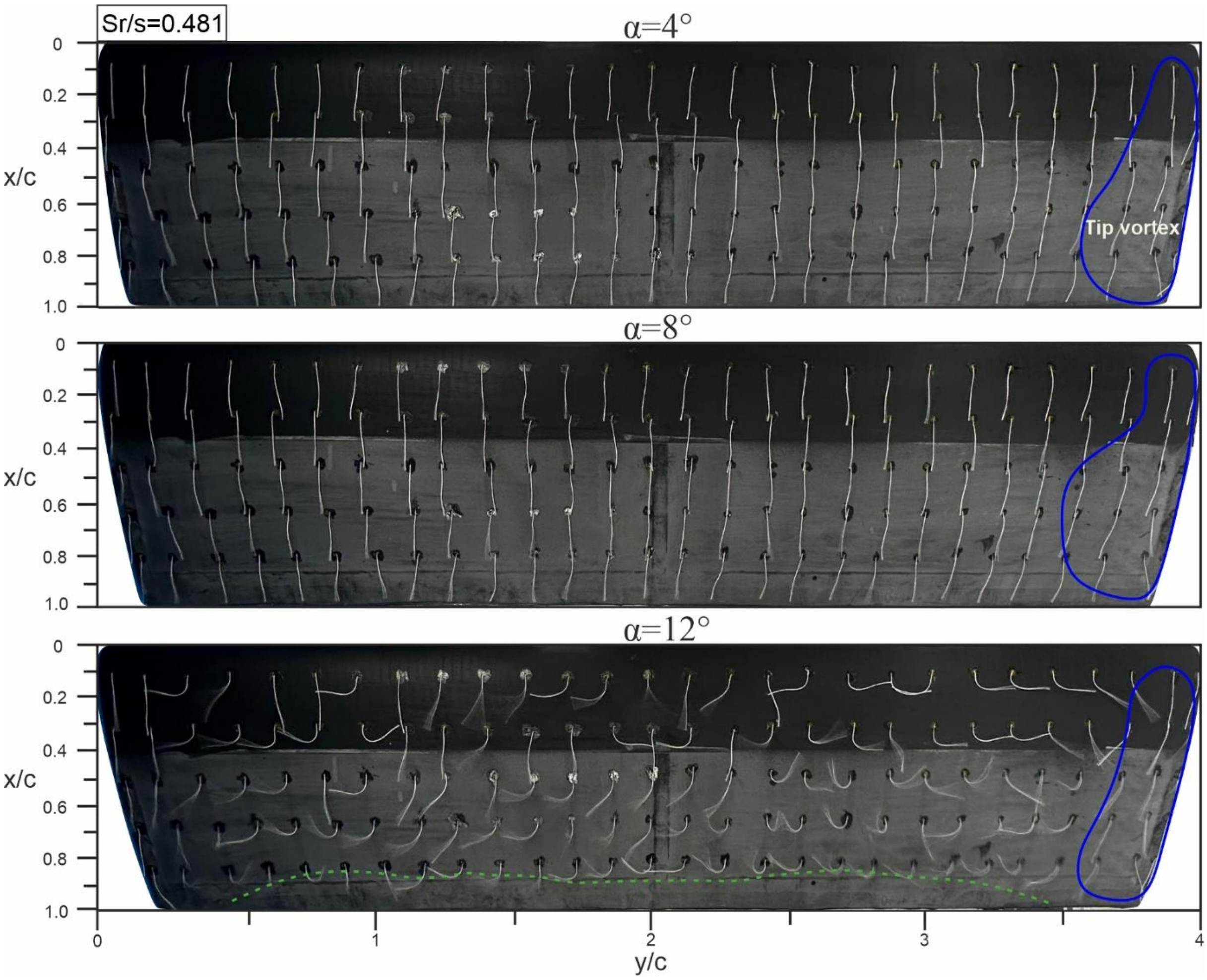

Figure 4.7. Tuft visualization of Sr/s = 0.481 model at α = 4°, 8° and 12°

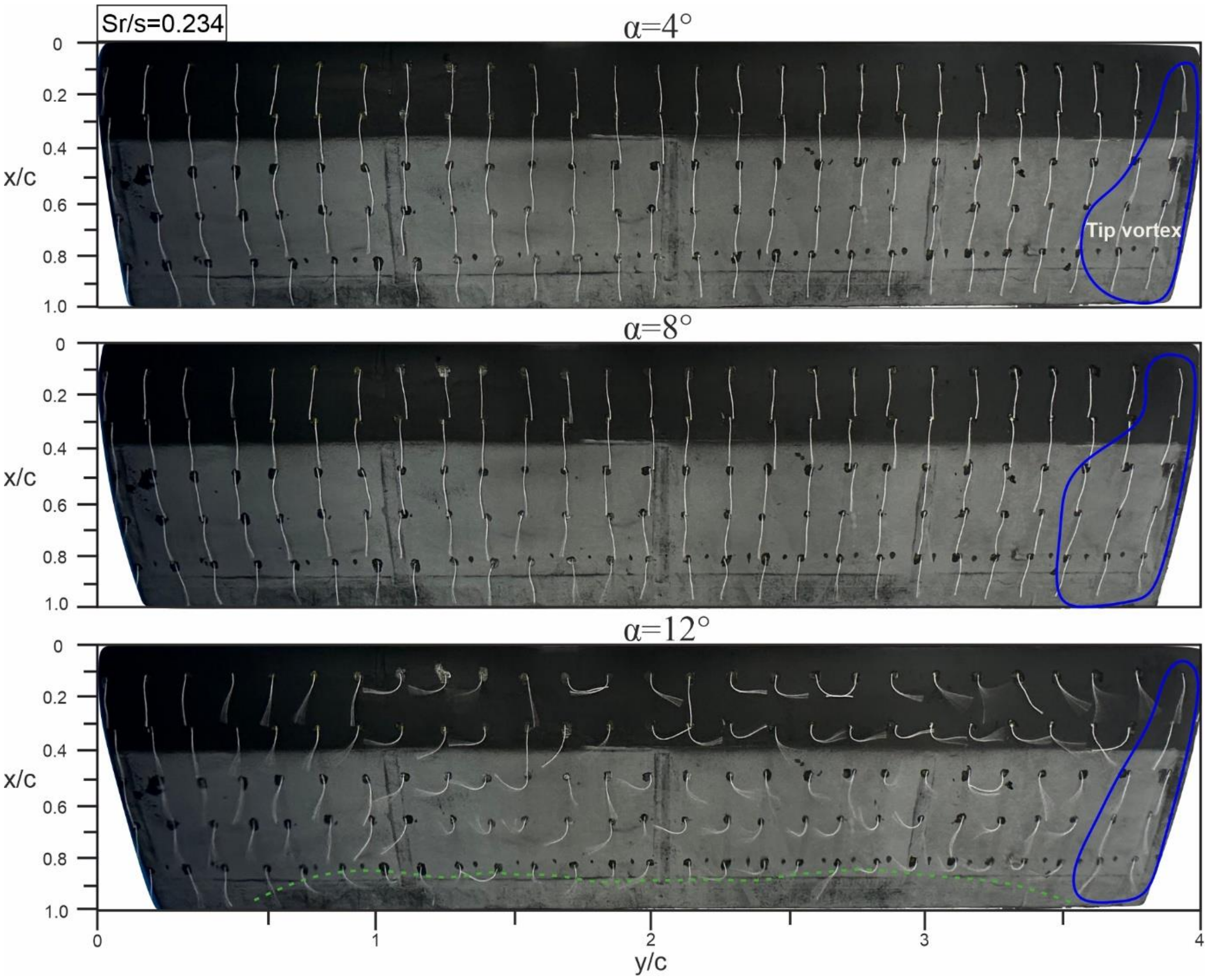

Figure 4.8. Tuft visualization of Sr/s = 0.234 model at α = 4°, 8° and 12°

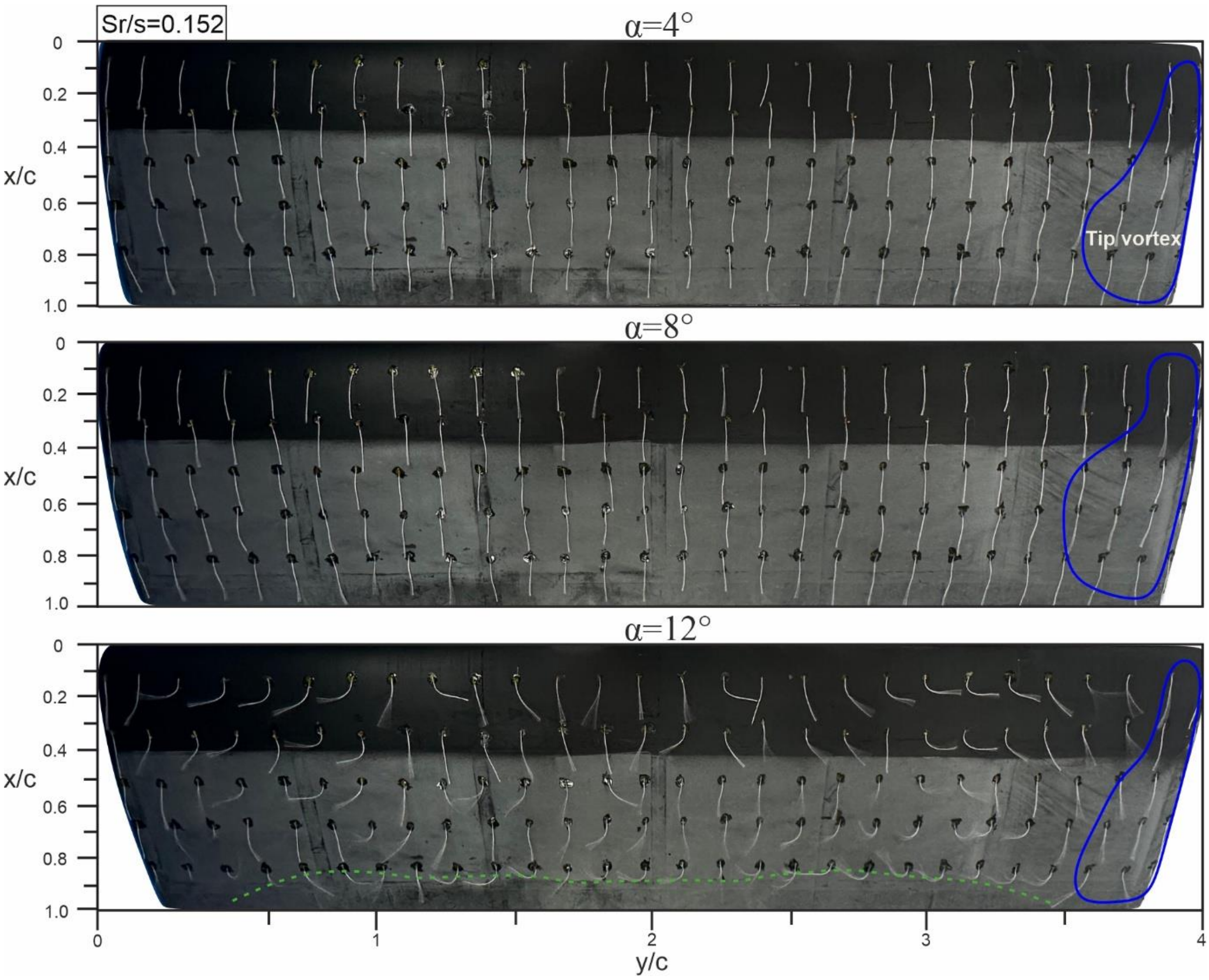

Figure 4.9. Tuft visualization of Sr/s = 0.152 model at α = 4°, 8° and 12°

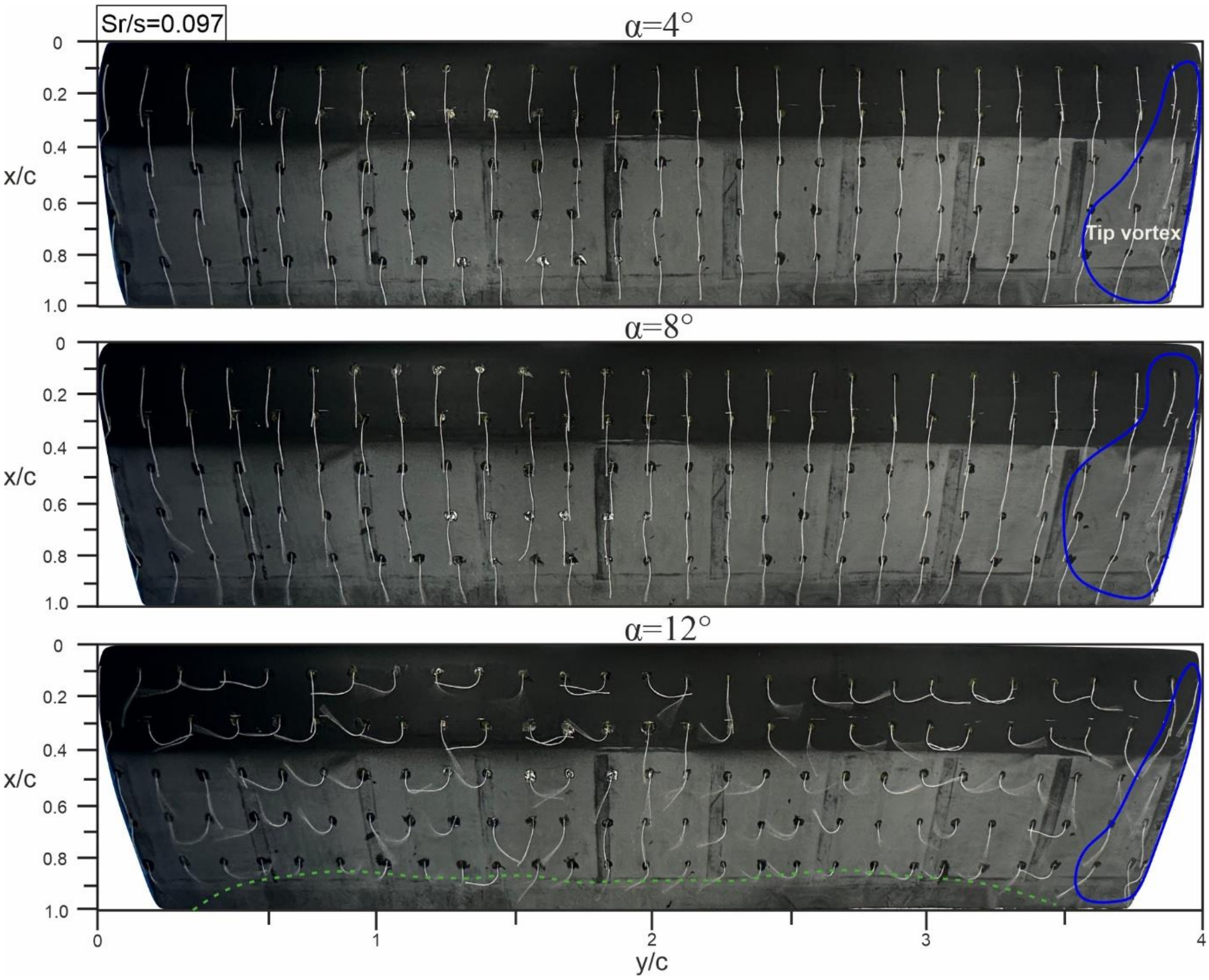

Figure 4.10. Tuft visualization of Sr/s = 0.097 model at α = 4°, 8° and 12°

5. CONCLUSIONS

This study experimentally investigated the aerodynamic effects of partially flexible surfaces applied to a finite NACA 0018 airfoil operating under low Reynolds number conditions ($3 \times 10^4 \leq Re \leq 10 \times 10^4$). The primary objective was to enhance aerodynamic efficiency, particularly in low-speed flight regimes typical of UAVs, by delaying flow separation and mitigating the adverse effects of LSBs.

Through comparative wind tunnel tests, the performance of four flexible wing models with varying spanwise flexibility ratios (Sr/s = 0.481, 0.234, 0.152, and 0.097) was evaluated against a rigid baseline airfoil. The results revealed that partial flexibility significantly improved the lift coefficient (C_L) and delayed stall onset, with the most pronounced benefits observed at the lower end of the tested Reynolds number range. For instance, at $Re = 3 \times 10^4$, the model with the highest flexibility ratio (Sr/s = 0.481) exhibited optimal performance, delaying the stall angle from 2.5° to 7° and increasing the maximum lift coefficient ($C_{L,\,max}$) while simultaneously reducing the size of the LSB. For the wing models with flexible surface ratios of Sr/s = 0.481 and Sr/s = 0.234, the maximum lift coefficient (CL) was achieved with a notable enhancement in lift performance compared to the rigid wing, corresponding to increases of 458% and 536% in maximum CL, respectively. Qualitative flow visualization, including surface oil and tuft methods, confirmed that the flexible membrane effectively suppressed early flow separation, helping to maintain attached flow over a broader range of angles of attack. However, the aerodynamic advantages of flexibility were observed to diminish as the Reynolds number increased, with performance approaching that of the rigid airfoil beyond $Re = 7.5 \times 10^4$.

These findings underscore that the spanwise extent of the flexible region critically influences the aerodynamic gains, with wings possessing larger flexible surface ratios leading to smoother flow transitions and greater lift-to-drag ratios. In conclusion, this research demonstrates the effectiveness of partial surface flexibility as a low-cost, lightweight, and energy-efficient passive flow control technique. The results contribute valuable practical insights for the design of flexible wings for small-scale UAV applications, offering a compelling alternative to more complex and energy-intensive active flow control methods.

6. RECOMMENDATIONS

While the current study has demonstrated the aerodynamic benefits of partially flexible surfaces under low Reynolds number conditions, there remain several directions for future investigation to further enhance the understanding and practical implementation of this concept.

Firstly, integrating CFD and fluid-structure interaction (FSI) simulations with experimental findings could offer a more comprehensive understanding of unsteady flow behavior and membrane deformation. Such analyses would help reveal detailed flow-field mechanisms that are difficult to capture through visualization techniques alone.

Secondly, the dynamic behavior of flexible surfaces under transient flow conditions, such as gust response, oscillatory inputs, or time-varying angles of attack, should be explored. Investigating how partial flexibility behaves in real flight scenarios can provide insights into structural fatigue, long-term performance stability, and responsiveness.

Moreover, future work could examine alternative flexible materials with varying stiffness, thickness, or damping properties to optimize the balance between aerodynamic performance and structural integrity. The implementation of smart materials or adaptive morphing skins may enable active control of flexibility in real time, further improving maneuverability and efficiency.

Lastly, expanding the study to different airfoil geometries, higher Reynolds number regimes, and three-dimensional flight conditions such as pitching or rolling maneuvers will make the findings more generalizable to a wider range of UAV and MAV applications.

REFERENCES

[1] M. Gaster, “The structure and behavior of separation bubbles,” 1967. https://reports.aerade.cranfield.ac.uk/handle/1826.2/2862

[2] M. Ol, B. McCauliffe, E. Hanff, U. Scholz, and C. Kaehler, “Comparison of laminar separation bubble measurements on a low Re airfoil in three facilities,” 36th AIAA Fluid Dynamics Conference and Exhibit, Jun. 2005, doi: 10.2514/6.2005-5149.

[3] W. B. Roberts, “Calculation of laminar separation bubbles and their effect on airfoil performance,” AIAA Journal, vol. 18, no. 1, pp. 25–31, Jan. 1980, doi: 10.2514/3.50726.

[4] M. ALAM and N. D. SANDHAM, “Direct numerical simulation of ‘short’ laminar separation bubbles with turbulent reattachment,” Journal of Fluid Mechanics, vol. 410, pp. 1–28, 2000. doi:10.1017/S0022112099008976

[5] R. HAIN, C. J. KÄHLER, and R. RADESPIEL, “Dynamics of laminar separation bubbles at low-Reynolds-number aerofoils,” Journal of Fluid Mechanics, vol. 630, pp. 129–153, 2009. doi:10.1017/S0022112009006661

[6] C. E. Toppings and S. Yarusevych, “Spontaneous laminar separation bubble bursting on an airfoil,” AIAA Journal, pp. 1–10, Nov. 2024, doi: 10.2514/1.j064510.

[7] G. Neretti, “Active flow control by using plasma actuators,” in InTech eBooks, 2016. doi: 10.5772/62720.

[8] D. S. N. Bharghava, T. Jana, and M. Kaushik, “A survey on synthetic jets as active flow control,” Aerospace Systems, vol. 7, no. 3, pp. 435–451, May 2024, doi: 10.1007/s42401-024-00301-5.

[9] P. Kumar, H. Poonia, and L. Ali, “Insight into the dynamics of active and passive controls over the measurement of thermal conductivity of nanofluids subject to magnetic field and thermal radiation through the stretching surface,” Numerical Heat Transfer Part a Applications, pp. 1–16, Oct. 2023, doi: 10.1080/10407782.2023.2269475.

[10] T. Durhasan, “Passive Flow Control over an Airfoil by Control Rod at Low Re,” Journal of Applied Fluid Mechanics, vol. 13, no. 6, pp. 1819–1833, 2020, doi: 10.47176/jafm.13.06.31087.

[11] M. Akhlaghi, S. R. Mirmotahari, F. Ghafoorian, and M. Mehrpooya, “Numerical Study of Control Rod’s Cross-Section Effects on the Aerodynamic Performance of Savonius Vertical Axis Wind Turbine with Various Installation Positions at Suction Side,” Iranian Journal of Science and Technology Transactions of Mechanical Engineering, vol. 48, no. 4, pp. 2143–2165, Apr. 2024, doi: 10.1007/s40997-024-00770-1.

[12] S.-J. Lee, H.-C. Lim, M. Han, and S. S. Lee, “Flow control of circular cylinder with a V-grooved micro-riblet film,” Fluid Dynamics Research, vol. 37, no. 4, pp. 246–266, Jul. 2005, doi: 10.1016/j.fluiddyn.2005.05.002.

[13] T. Suresh, P. Flaszynski, A. R. Carpio, M. Kurowski, M. Piotrowicz, and O. Szulc, “Aeroacoustic effect of boundary layer separation control by rod vortex generators on the DU96-W-180 airfoil,” Journal of Fluids and Structures, vol. 127, p. 104133, May 2024, doi: 10.1016/j.jfluidstructs.2024.104133.

[14] R. Zhang et al., “Passive flow control technique for enhancing power efficiency of vertical-axis wind turbines: Leading-edge slot structure,” Journal of Ocean Engineering and Science, May 2025, doi: 10.1016/j.joes.2025.05.002.

[15] M. Gad-El-Hak, “Flow control,” Applied Mechanics Reviews, vol. 42, no. 10, pp. 261–293, Oct. 1989, doi: 10.1115/1.3152376.

[16] R. Smith and J. Wright, “Simulation of the viscous aeroelastic response of a membrane airfoil to a harmonically varying freestream,” 38th Aerospace Sciences Meeting and Exhibit, Jan. 2001, doi: 10.2514/6.2001-857.

[17] A. Song et al., “Aeromechanics of Membrane Wings with Implications for Animal Flight,” AIAA Journal, vol. 46, no. 8, pp. 2096–2106, Jul. 2008, doi: 10.2514/1.36694.

[18] W. Shyy, M. Berg, and D. Ljungqvist, “Flapping and flexible wings for biological and micro air vehicles,” Progress in Aerospace Sciences, vol. 35, no. 5, pp. 455–505, Jul. 1999, doi: 10.1016/s0376-0421(98)00016-5.

[19] B. Béguin and C. Breitsamter, “Effects of membrane pre-stress on the aerodynamic characteristics of an elasto-flexible morphing wing,” Aerospace Science and Technology, vol. 37, pp. 138–150, Jun. 2014, doi: 10.1016/j.ast.2014.05.005.

[20] Y. Liu, L. Zuo, and J. Wang, “Effects of flexibility on aerodynamic performance of delta wings with different sweep angles,” Science China Physics Mechanics and Astronomy, vol. 53, no. 5, pp. 915–922, Apr. 2010, doi: 10.1007/s11433-010-0167-1.

[21] S. Yarusevych, P. E. Sullivan, and J. G. Kawall, “Effect of acoustic excitation amplitude on airfoil boundary layer and wake development,” AIAA Journal, vol. 45, no. 4, pp. 760–771, Mar. 2007, doi: 10.2514/1.25439.

[22] T. Xia, H. Dong, L. Yang, S. Liu, and Z. Jin, “Investigation on flow structure and aerodynamic characteristics over an airfoil at low Re—A review,” AIP Advances, vol. 11, no. 5, May 2021, doi: 10.1063/5.0044717.

[23] C. Badrya, B. Govindarajan, and I. Chopra, “Basic understanding of unsteady airfoil aerodynamics at low Re,” 2018 AIAA Aerospace Sciences Meeting, Jan. 2018, doi: 10.2514/6.2018-2061.

[24] https://eaglepubs.erau.edu/introductiontoaerospaceflightvehicles/chapter/mach-number-and-reynolds-number/

[25] B. F. Klose, G. R. Spedding, and G. B. Jacobs, "Flow separation, instability and transition to turbulence on a cambered airfoil at Re 20 000," Journal of Fluid Mechanics, vol. 1009, p. A9, 2025. doi:10.1017/jfm.2025.212

[26] https://eaglepubs.erau.edu/introductiontoaerospaceflightvehicles/chapter/introduction-to-boundary-layers/

[27] D. Borgmann, S. Hosseinverdi, J. Little, and H. Fasel, "Experimental and numerical investigations of transition in a pressure-gradient-induced laminar separation bubble," Journal of Fluid Mechanics, vol. 1007, p. A23, 2025. doi:10.1017/jfm.2025.43

[28] H. Sturm, G. Dumstorff, P. Busche, D. Westermann, and W. Lang, "Boundary layer separation and reattachment detection on airfoils by thermal flow sensors," Sensors, vol. 12, no. 11, pp. 14292–14306, Oct. 2012, doi: 10.3390/s121114292.

[29] D. De Rosa, S. Hein, J. A. Franco, and F. Tocci, "Stability Analysis of laminar separation bubbles on airfoils," AIAA SCITECH 2022 Forum, Jan. 2024, doi: 10.2514/6.2024-1358.

[30] Sturm, H., Dumstorff, G., Busche, P., Westermann, D., & Lang, W. (2012). Boundary layer separation and reattachment detection on airfoils by thermal flow sensors. Sensors, 12(11), 14292–14306. https://doi.org/10.3390/s121114292

[31]https://eaglepubs.erau.edu/introductiontoaerospaceflightvehicles/chapter/finite-wing-characteristics/

[32]C. E. Toppings and S. Yarusevych, "Laminar separation bubble formation and bursting on a finite wing," Journal of Fluid Mechanics, vol. 986, May 2024, doi: 10.1017/jfm.2024.321.

[33]C. E. Toppings and S. Yarusevych, "Structure and dynamics of a laminar separation bubble near a wing root: towards reconstructing the complete LSB topology on a finite wing," Journal of Fluid Mechanics, vol. 944, Jun. 2022, doi: 10.1017/jfm.2022.460.

[34]https://eaglepubs.erau.edu/introductiontoaerospaceflightvehicles/chapter/maximum-lift-stalling-spinning/

[35] R. F. Huang, J. Y. Wu, J. H. Jeng, and R. C. Chen, "Surface flow and vortex shedding of an impulsively started wing," Journal of Fluid Mechanics, vol. 441, pp. 265–292, Aug. 2001, doi: 10.1017/s002211200100489x.

[36] A. E. Panah and J. Buchholz, "Vortex shedding and wake structure of a plunging wing," 50th AIAA Aerospace Sciences Meeting Including the New Horizons Forum and Aerospace Exposition, Jan. 2012, doi: 10.2514/6.2012-913.

[37] J. D. Anderson, "Ludwig Prandtl's Boundary Layer," Physics Today, vol. 58, no. 12, pp. 42–48, Dec. 2005, doi: 10.1063/1.2169443.

[38] P. R. Ashill, J. L. Fulker, and K. C. Hackett, "A review of recent developments in flow control," The Aeronautical Journal, vol. 109, no. 1095, pp. 205–232, May 2005, doi: 10.1017/s0001924000005200.

[39] Othman, A. K., Zekry, D. A., Saro-Cortes, V., Lee, K. J. "., & Wissa, A. A. (2023). Aerial and aquatic biological and bioinspired flow control strategies. Communications Engineering,

[40] B. Yagiz, O. Kandil, and Y. V. Pehlivanoglu, “Drag minimization using active and passive flow control techniques,” Aerospace Science and Technology, vol. 17, no. 1, pp. 21–31, Mar. 2011, doi: 10.1016/j.ast.2011.03.003.

[41] J. S. Delnero, J. M. Di Leo, M. E. Camocardi, M. A. Martinez, and J. L. C. Lerner, “Experimental study of vortex generators effects on low Re airfoils in turbulent flow,” International Journal of Aerodynamics, vol. 2, no. 1, p. 50, Jan. 2012, doi: 10.1504/ijad.2012.046539.

[42] H. Wang et al., “Effects of leading edge slat on flow separation and aerodynamic performance of wind turbine,” Energy, vol. 182, pp. 988–998, Jun. 2019, doi: 10.1016/j.energy.2019.06.096.

[43] https://zenithair.net/high-lift-design-2/

[44] R. Belamadi, A. Djemili, A. Ilinca, and R. Mdouki, “Aerodynamic performance analysis of slotted airfoils for application to wind turbine blades,” Journal of Wind Engineering and Industrial Aerodynamics, vol. 151, pp. 79–99, Feb. 2016, doi: 10.1016/j.jweia.2016.01.011.

[45] R. H. Liebeck, “Design of subsonic airfoils for high lift,” Journal of Aircraft, vol. 15, no. 9, pp. 547–561, Sep. 1978, doi: 10.2514/3.58406.

[46] V. Shukla and A. K. Kaviti, “Performance evaluation of profile modifications on straight-bladed vertical axis wind turbine by energy and Spalart Allmaras models,” Energy, vol. 126, pp. 766–795, Mar. 2017, doi: 10.1016/j.energy.2017.03.071.

[47] http://www.insideracingtechnology.com/tech104gurney.htm

[48] M. S. Genç, K. Koca, H. Demir, and H. H. Açıkel, “Traditional and new types of passive flow control techniques to pave the way for high maneuverability and low structural weight for UAVs and MAVs,” in IntechOpen eBooks, 2020. doi: 10.5772/intechopen.90552.

[49] M. S. Genç, K. Koca, and H. H. Açikel, “Investigation of pre-stall flow control on wind turbine blade airfoil using roughness element,” Energy, vol. 176, pp. 320–334, Apr. 2019, doi: 10.1016/j.energy.2019.03.179.

[50] T. J. Mueller and J. D. DeLaurier, “AERODYNAMICS OFSMALLVEHICLES,” Annual Review of Fluid Mechanics, vol. 35, no. 1, pp. 89–111, Dec. 2002, doi: 10.1146/annurev.fluid.35.101101.161102.

[51] S. Arbós-Torrent, B. Ganapathisubramani, and R. Palacios, “Leading- and trailing-edge effects on the aeromechanics of membrane aerofoils,” Journal of Fluids and Structures, vol. 38, pp. 107–126, Feb. 2013, doi: 10.1016/j.jfluidstructs.2013.01.005.

[52] D. Hefeng, W. Chenxi, L. Shaobin, and S. X. Zhen, “Numerical research on segmented flexible airfoils considering fluid-structure interaction,” Procedia Engineering, vol. 99, pp. 57–66, Jan. 2015, doi: 10.1016/j.proeng.2014.12.508.

[53] J. H. Moghimi Esfandabadi, H. Attar, K. Karbasi Shargh, M. Javareshakian, S. Ghasemi ve M. Moghimi, “A Review of Passive Control Flow Past UAV Wings,” in Proc. 2023 2nd International Engineering Conference on Electrical, Energy, and Artificial Intelligence (EICEEAI), Dec. 2023, doi: 10.1109/EICEEAI60672.2023.10590150.

[54] N. V. T. Gopinathan and N. M. Ganesh, "Passive Flow Control over Naca0012 Aerofoil using Vortex Generators," International Journal of Engineering Research And, vol. V4, no. 09, Sep. 2015, doi: 10.17577/ijertv4is090634.

[55] "PDF | Design of Passive Flow Control Device Derived from Bird Wing Aerodynamics. | ID: 1831cw88f | Tufts Digital Library." https://dl.tufts.edu/concern/pdfs/1831cw88f

[56] K. Al-Jaburi, "Passive flow control of Rotary-Wing and Fixed-Wing aircraft airfoils via Surface-Based trapped vortex generators," 2019. doi: 10.22215/etd/2019-13461.

[57] S. N. J. Y. S. G., "A Review on Active and Passive Flow Control Techniques", IJRMEE, vol. 3, no. 4, pp. 01–06, Apr. 2016.

[58] P. Tewes, "Application of active flow control to a finite swept wing," 2015. doi: 10.14279/depositonce-4921.

[59] J. A. Ekaterinaris, "Active flow control of wing separated flow," in Proc. ASME Fluids Engineering Division Summer Meeting (FEDSM), Paper no. FEDSM2003-45237, Honolulu, HI, USA, Jun. 2003, pp. 2727–2735. doi: 10.1115/FEDSM2003-45237.

[60] D. Schatzman, J. Wilson, E. Arad, A. Seifert, and T. Shtendel, "Drag-Reduction mechanisms of Suction-and-Oscillatory-Blowing flow control," AIAA Journal, vol. 52, no. 11, pp. 2491–2505, Sep. 2014, doi: 10.2514/1.j052903.

[61] B. Li, X. Meng, S. Yin, W. Hui, and H. Li, "Flow Separation Control over an Airfoil Using Plasma Co-Flow Jet," AIAA Journal, vol. 60, no. 4, pp. 2195–2206, Oct. 2021, doi: 10.2514/1.j060911.

[62] H. Zong, M. Chiatto, M. Kotsonis, and L. De Luca, "Plasma synthetic jet actuators for active flow control," Actuators, vol. 7, no. 4, p. 77, Nov. 2018, doi: 10.3390/act7040077.

[63] G. Zhao, Q. Zhao, and X. Chen, "Wind-tunnel tests of synthetic jet control effects on airfoil flow separation," Scientific Reports, vol. 12, no. 1, Dec. 2022, doi: 10.1038/s41598-022-19642-2.

[64] M. Jahanmiri, Active Flow Control: A Review, Research Report 2010:12, Division of Fluid Dynamics, Department of Applied Mechanics, Chalmers University of Technology, Gothenburg, Sweden, 2010.

[65] J. W. Zimmerman, A. Palla, D. L. Carroll, G. Hristov, and P. J. Ansell, "Plasma Actuator with Arc Breakdown in a Magnetic Field for Active Flow Control Applications," 34th AIAA Plasmadynamics and Lasers Conference, Jun. 2017, doi: 10.2514/6.2017-3477.

[66] L. Huang, P. G. Huang, R. P. LeBeau, and T. Hauser, "Numerical study of blowing and suction control mechanism on NACA0012 Airfoil," Journal of Aircraft, vol. 41, no. 5, pp. 1005–1013, Sep. 2004, doi: 10.2514/1.2255.

[67] G. Fahland et al., "Investigation of blowing and suction for turbulent flow control on airfoils," AIAA Journal, vol. 59, no. 11, pp. 4422–4436, Jul. 2021, doi: 10.2514/1.j060211.

[68] C. He, T. C. Corke, and M. P. Patel, “Plasma flaps and slats: an application of weakly ionized plasma actuators,” Journal of Aircraft, vol. 46, no. 3, pp. 864–873, May 2009, doi: 10.2514/1.38232.

[69] E. Moreau, A. Debien, J.-M. Breux, and N. Benard, “Control of a turbulent flow separated at mid-chord along an airfoil with DBD plasma actuators,” Journal of Electrostatics, vol. 83, pp. 78–87, Aug. 2016, doi: 10.1016/j.elstat.2016.08.005.

[70] A. Glezer, “Some aspects of aerodynamic flow control using synthetic-jet actuation,” Philosophical Transactions of the Royal Society a Mathematical Physical and Engineering Sciences, vol. 369, no. 1940, pp. 1476–1494, Mar. 2011, doi: 10.1098/rsta.2010.0374.

[71] M. G. De Giorgi, C. G. De Luca, A. Ficarella, and F. Marra, “Comparison between synthetic jets and continuous jets for active flow control: Application on a NACA 0015 and a compressor stator cascade,” Aerospace Science and Technology, vol. 43, pp. 256–280, Mar. 2015, doi: 10.1016/j.ast.2015.03.004.

[72] C. Lee, G. Hong, Q. P. Ha, and S. G. Mallinson, “A piezoelectrically actuated micro synthetic jet for active flow control,” Sensors and Actuators a Physical, vol. 108, no. 1–3, pp. 168–174, Nov. 2003, doi: 10.1016/s0924-4247(03)00267-x.

[73] J. Kim and I. Lee, “Numerical simulation and analysis of flow control using electromagnetic forcing,” in 35th Aerospace Sciences Meeting and Exhibit, AIAA Paper 1997-1797, Jan. 1997. doi: 10.2514/6.1997-1797

[74] J. Donovan, L. Kral, and A. Cary, “Characterization of a Lorentz force actuator,” in 4th Shear Flow Control Conference, Snowmass Village, CO, USA, 29 June–2 July 1997, AIAA Paper 1997-1918, doi: 10.2514/6.1997-1918.

[75] S. E. James, A. Suryan, J. J. Sebastian, A. Mohan, and H. D. Kim, “Comparative study of boundary layer control around an ordinary airfoil and a high lift airfoil with secondary blowing,” Computers & Fluids, vol. 164, pp. 50–63, Mar. 2017, doi: 10.1016/j.compfluid.2017.03.012.

[76] K. Koca, M. Serdar Genç, and H. Hakan Açikel, “Experimental Investigation of Surface Roughness Effect over Wind Turbine Airfoil,” 2016.

[77] M. S. Genç, K. Koca, and H. H. Açikel, “Investigation of pre-stall flow control on wind turbine blade airfoil using roughness element,” Energy, vol. 176, pp. 320–334, Apr. 2019, doi: 10.1016/j.energy.2019.03.179.

[78] T. Mu, R. Zhang, H. Xu, Y. Zheng, Z. Fei, and J. Li, “Study on improvement of hydraulic performance and internal flow pattern of the axial flow pump by groove flow control technology,” Renew Energy, vol. 160, pp. 756–769, Nov. 2020, doi: 10.1016/j.renene.2020.06.145.

[79] S. H. Seo and C. H. Hong, “Performance improvement of airfoils for wind blade with the groove,” Int J Green Energy, vol. 13, no. 1, pp. 34–39, Jan. 2016, doi: 10.1080/15435075.2014.910777.

[80] B. L. Storms and C. S. Jang, “Lift enhancement of an airfoil using a Gurney flap and vortex generators,” J Aircr, vol. 31, no. 3, pp. 542–547, 1994, doi: 10.2514/3.46528.

[81] K. Yee, W. Joo, and D.-H. Lee, “Aerodynamic performance analysis of a Gurney flap for rotorcraft application,” Journal of Aircraft, vol. 44, no. 3, pp. 1003–1014, May 2007, doi: 10.2514/1.26868.

[82] M. Chandrasekhara, P. Martin, and C. Tung, “Compressible Dynamic Stall Performance of a Variable Droop Leading Edge Airfoil with a Gurney Flap,” 42nd AIAA Aerospace Sciences Meeting and Exhibit, Jan. 2004, doi: 10.2514/6.2004-41.

[83] M. S. Genç, Ü. Kaynak, and G. D. Lock, “Flow over an aerofoil without and with a leading-edge slat at a transitional Re,” Proceedings of the Institution of Mechanical Engineers Part G Journal of Aerospace Engineering, vol. 223, no. 3, pp. 217–231, Feb. 2009, doi: 10.1243/09544100jaero434.

[84] M. Schramm, B. Stoevesandt, and J. Peinke, “Simulation and Optimization of an Airfoil with Leading Edge Slat,” Journal of Physics Conference Series, vol. 753, p. 022052, Sep. 2016, doi: 10.1088/1742-6596/753/2/022052.

[85] S. Mishra and J. Baeder, “Coupled CFD/CSD prediction of the effects of leading edge slat on rotor performance,” Proceedings of the 72nd American Helicopter Society Annual Forum, West Palm Beach, FL, USA, May 2016. doi: 10.13140/2.1.2255.0409

[86] J. M. Mendoza, T. F. Brooks, and W. M. Humphreys, “An aeroacoustic study of a leading EDGE Slat configuration,” International Journal of Aeroacoustics, vol. 1, no. 3, pp. 241–274, Sep. 2002, doi: 10.1260/147547202320962583.

[87] H. Mueller-Vahl, G. Pechlivanoglou, C. N. Nayeri, and C. O. Paschereit, “Vortex Generators for Wind Turbine Blades: A Combined Wind Tunnel and Wind Turbine Parametric Study,” in Proc. ASME Turbo Expo 2012: Turbine Technical Conference and Exposition, Copenhagen, Denmark, June 2012, Paper No. GT2012-69197.

[88] P. Kundu, A. Sarkar, and V. Nagarajan, “Improvement of performance of S1210 hydrofoil with vortex generators and modified trailing edge,” Renewable Energy, vol. 142, pp. 643–657, May 2019, doi: 10.1016/j.renene.2019.04.148.

[89] H. Wang, B. Zhang, Q. Qiu, and X. Xu, “Flow control on the NREL S809 wind turbine airfoil using vortex generators,” Energy, vol. 118, pp. 1210–1221, Nov. 2016, doi: 10.1016/j.energy.2016.11.003.

[90] J. Piquee, I. López, C. Breitsamter, R. Wüchner, and K.-U. Bletzinger, “Aerodynamic Characteristics of an Elasto-Flexible Membrane Wing based on Experimental and Numerical Investigations,” 2018 Applied Aerodynamics Conference, Jun. 2018, doi: 10.2514/6.2018-3338.

[91] H. Demir and M. S. Genç, “An experimental investigation of laminar separation bubble formation on flexible membrane wing,” European Journal of Mechanics - B/Fluids, vol. 65, pp. 326–338, Jun. 2017, doi: 10.1016/j.euromechflu.2017.05.010.

[92] P. Rojratsirikul, Genc, Z. Wang, and I. Gursul, "Flow-induced vibrations of low aspect ratio rectangular membrane wings," Journal of Fluids and Structures, vol. 27, no. 8, pp. 1296–1309, Jul. 2011, doi: 10.1016/j.jfluidstructs.2011.06.007.

[93] M. S. Genç, M. Özden, H. H. Açikel, H. Demir, and I. Isabekov, "Unsteady flow over flexible wings at different low Re," EPJ Web of Conferences, vol. 114, p. 02030, Jan. 2016, doi: 10.1051/epjconf/201611402030.

[94] Q. Guo, X. He, Z. Wang, and J. Wang, "Effects of wing flexibility on aerodynamic performance of an aircraft model," Chinese Journal of Aeronautics, vol. 34, no. 9, pp. 133–142, Mar. 2021, doi: 10.1016/j.cja.2021.01.012.

[95] A. M. DeLuca, M. F. Reeder, M. V. Ol, J. Freeman, I. Bautista, and M. Simonich, "Experimental Investigation into the Aerodynamic Properties of a Flexible and Rigid Wing Micro Air Vehicle," in Proc. 24th AIAA Aerodynamic Measurement Technology and Ground Testing Conference, Portland, OR, USA, Jun. 28 – Jul. 1, 2004, AIAA Paper 2004-2396.

[96]A. Maqsood, "FLEXIBLE WING AERODYNAMICS AT LOW RE," Nust, May 2014, [Online]. Available: https://www.academia.edu/3004214/FLEXIBLE_WING_AERODYNAMICS_AT_LOW_REYNOLDS_NUMBERS

[97] E. V. Laitone, "Wind tunnel tests of wings at Re below 70 000," Experiments in Fluids, vol. 23, no. 5, pp. 405–409, Nov. 1997, doi: 10.1007/s003480050128.

[98] J. M. Akkala, A. E. Panah, and J. H. J. Buchholz, "Vortex dynamics and performance of flexible and rigid plunging airfoils," Journal of Fluids and Structures, vol. 54, pp. 103–121, Dec. 2014, doi: 10.1016/j.jfluidstructs.2014.10.013.

[99] P. Rojratsirikul, Z. Wang, and I. Gursul, "Unsteady aerodynamics of low aspect ratio membrane wings," 50th AIAA Aerospace Sciences Meeting Including the New Horizons Forum and Aerospace Exposition, Jan. 2010, doi: 10.2514/6.2010-729.

[100] A. Timpe, Z. Zhang, J. Hubner, and L. Ukeiley, "Passive flow control by membrane wings for aerodynamic benefit," Experiments in Fluids, vol. 54, no. 3, Feb. 2013, doi: 10.1007/s00348-013-1471-0.

[101] D. J. Cleaver, D. E. Calderon, Z. Wang, and I. Gursul, "Lift enhancement through flexibility of plunging wings at low Re," Journal of Fluids and Structures, vol. 64, pp. 27–45, Apr. 2016, doi: 10.1016/j.jfluidstructs.2016.04.004.

[102] R. E. Gordnier and P. J. Attar, "Impact of flexibility on the aerodynamics of an aspect ratio two membrane wing," Journal of Fluids and Structures, vol. 45, pp. 138–152, Jan. 2014, doi: 10.1016/j.jfluidstructs.2013.10.004.

[103] S. Greenhalgh, H. Curtiss Jr, and B. Smith, "Aerodynamic properties of a two-dimensional inextensible flexible airfoil," 2018 Applied Aerodynamics Conference, Jul. 1983, doi: 10.2514/6.1983-1796.

[104] H. Hu, A. G. Kumar, G. Abate, and R. Albertani, "An experimental investigation on the aerodynamic performances of flexible membrane wings in flapping flight," Aerospace Science and Technology, vol. 14, no. 8, pp. 575–586, May 2010, doi: 10.1016/j.ast.2010.05.003.

[105] W. Shyy et al., “Computational aerodynamics of low Re plunging, pitching and flexible wings for MAV applications,” Acta Mechanica Sinica, vol. 24, no. 4, pp. 351–373, Jul. 2008, doi: 10.1007/s10409-008-0164-z.

[106] G. Li, B. C. Khoo, and R. K. Jaiman, “Computational Aeroelasticity of Flexible Membrane Wings at Moderate Re,” presented at the AIAA SciTech Forum, Orlando, FL, USA, Jan. 2020, Paper No. AIAA 2020-2036. doi: 10.2514/6.2020-2036

[107] C. -k. Kang, H. Aono, C. E. S. Cesnik, and W. Shyy, “Effects of flexibility on the aerodynamic performance of flapping wings,” Journal of Fluid Mechanics, vol. 689, pp. 32–74, Nov. 2011, doi: 10.1017/jfm.2011.428.

[108] M. Tamai, J. Murphy, and H. Hu, “An experimental study of flexible membrane airfoils at Low Re,” 45th AIAA Aerospace Sciences Meeting and Exhibit, Jan. 2008, doi: 10.2514/6.2008-580.

[109] H. H. Açıkel and M. S. Genç, “Control of laminar separation bubble over wind turbine airfoil using partial flexibility on suction surface,” Energy, vol. 165, pp. 176–190, Sep. 2018, doi: 10.1016/j.energy.2018.09.040.

[110] M. S. Genç, H. H. Açıkel, and K. Koca, “Effect of partial flexibility over both upper and lower surfaces to flow over wind turbine airfoil,” Energy Conversion and Management, vol. 219, p. 113042, Jun. 2020, doi: 10.1016/j.enconman.2020.113042.

[111] A. E. Eroğlu, T. Durhasan, J. R. Jafari, and İ. Karasu, “Experimental Investigation of Local Flexible Surface on Aerodynamic Effects for Finite Wing with NACA0018 Section,” Çukurova Üniversitesi Mühendislik Fakültesi Dergisi, vol. 40, no. 1, pp. 61–68, Mar. 2025, doi: 10.21605/cukurovaumfd.1665840.

[112] M. Mojtahedpoor and A. Naderi, “Numerical investigation of local flexible membranes effects on separated laminar and transient flows,” Indian Journal of Science and Technology, vol. 9, no. 48, Dec. 2016, doi: 10.17485/ijst/2016/v9i48/91729.

[113] W. Shyy, F. Klevebring, M. Nilsson, J. Sloan, B. Carroll, and C. Fuentes, “Rigid and flexible low Re airfoils,” Journal of Aircraft, vol. 36, no. 3, pp. 523–529, May 1999, doi: 10.2514/2.2487.

[114] Y. Abudaram, B. Stanford, and P. Ifju, “Wind tunnel testing of Load-Alleviating Membrane wings at Low Re,” 50th AIAA Aerospace Sciences Meeting Including the New Horizons Forum and Aerospace Exposition, Jan. 2009, doi: 10.2514/6.2009-1468.

[115] M. S. Genç, M. Özden, H. H. Açikel, H. Demir, and I. Isabekov, “Unsteady flow over flexible wings at different low Re,” EPJ Web of Conferences, vol. 114, p. 02030, Jan. 2016, doi: 10.1051/epjconf/201611402030.

[116] D. Hefeng, W. Chenxi, L. Shaobin, and S. X. Zhen, “Numerical research on segmented flexible airfoils considering fluid-structure interaction,” Procedia Engineering, vol. 99, pp. 57–66, Jan. 2015, doi: 10.1016/j.proeng.2014.12.508.

[117] B. Lou, S. Ye, G. Wang, and Z. Huang, “Numerical and experimental research of flow control on an NACA 0012 airfoil by local vibration,” Applied Mathematics and Mechanics, vol. 40, no. 1, pp. 1–12, Dec. 2018, doi: 10.1007/s10483-019-2404-8.

[118] P. Rojratsirikul, Z. Wang, and I. Gursul, “Effect of Pre-Strain and excess length on unsteady Fluid-Structure interactions of membrane airfoils,” 50th AIAA Aerospace Sciences Meeting Including the New Horizons Forum and Aerospace Exposition, Jan. 2009, doi: 10.2514/6.2009-578.

[119] J. B. Barlow, W. H. Rae Jr., and A. Pope, Low-Speed Wind Tunnel Testing, 3rd ed. Hoboken, NJ, USA: Wiley-Interscience, 1999.

[120] İ. Karasu, M. Özden, and M. S. Genç, “Performance Assessment of Transition Models for Three-Dimensional Flow over NACA4412 wings at Low Re,” Journal of Fluids Engineering, vol. 140, no. 12, Jun. 2018, doi: 10.1115/1.4040228.

[121] R. L. Maltby, Flow Visualization in Wind Tunnels Using Indicators, AGARDograph No. 70, North Atlantic Treaty Organization (NATO), Advisory Group for Aeronautical Research and Development, April 1962.

[122] M. S. H. Boutilier and S. Yarusevych, “Parametric study of separation and transition characteristics over an airfoil at low Re,” Experiments in Fluids, vol. 52, no. 6, pp. 1491–1506, Feb. 2012, doi: 10.1007/s00348-012-1270-z.

[123] K. Rogowski, R. F. Mikkelsen, J. Michna, and J. Wiśniewski, “Aerodynamic performance analysis of NACA 0018 airfoil at low Re in a low-turbulence wind tunnel,” Advances in Science and Technology – Research Journal, vol. 19, no. 2, pp. 136–150, Nov. 2024, doi: 10.12913/22998624/195556.